ESCOLA POLITÉCNICA
PROGRAMA DE PÓS-GRADUAÇÃO EM ENGENHARIA ELÉTRICA
MESTRADO EM ENGENHARIA ELÉTRICA

BERNARDO SERPA BORGES

SEMIDEFINITE PROGRAMMING SOLUTION TO THE ANALYSIS AND CONTROL PROBLEM OF A TORPEDO SHAPED AUTONOMOUS UNDERWATER VEHICLE

Porto Alegre
2018

Bernardo Serpa Borges

Semidefinite Programming Solution to the Analysis and Control Problem of a Torpedo Shaped Autonomous Underwater Vehicle

Porto Alegre - RS, Brazil
2018

Bernardo Serpa Borges

Semidefinite Programming Solution to the Analysis and Control Problem of a Torpedo Shaped Autonomous Underwater Vehicle

Masters dissertation presented to the Graduate Program in Electrical Engineering of the Pontifícia Universidade Católica do Rio Grande do Sul, as requisite to obtain Master's degree in Electrical Engineering.
Focus area: Signals, Systems and Information Technology
Research area: Automation and Systems.

Pontifícia Universidade do Rio Grande do Sul - PUCRS

School of Technology

Graduate Program in Electrical Engineering

Supervisor: Guilherme Araujo Pimentel

Porto Alegre - RS, Brazil

2018

Ficha Catalográfica

B732s Borges, Bernardo Serpa

Semidefinite Programming Solution to the Analysis and Control Problem of a Torpedo Shaped Autonomous Underwater Vehicle / Bernardo Serpa Borges . – 2018.

75 p.

Dissertação (Mestrado) – Programa de Pós-Graduação em Engenharia Elétrica, PUCRS.

Orientador: Prof. Dr. Guilherme Araujo Pimentel.

1. Autonomous Underwater Vehicle. 2. Semidefinite Optimization. 3. Linear Matrix Inequalities. 4. Differential Algebraic Representation. 5. Torpedo. I. Pimentel, Guilherme Araujo. II. Título.

Elaborada pelo Sistema de Geração Automática de Ficha Catalográfica da PUCRS
com os dados fornecidos pelo(a) autor(a).
Bibliotecária responsável: Salete Maria Sartori CRB-10/1363

Pontifícia Universidade Católica do Rio Grande do Sul
ESCOLA POLITÉCNICA
PROGRAMA DE PÓS-GRADUAÇÃO EM ENGENHARIA ELÉTRICA - PPGEE

SEMIDEFINITE PROGRAMMING SOLUTION TO THE ANALYSIS AND CONTROL PROBLEM OF A TORPEDO SHAPED AUTONOMOUS UNDERWATER VEHICLE

CANDIDATO: BERNARDO SERPA BORGES

Esta Dissertação de Mestrado foi julgada para obtenção do título de MESTRE EM ENGENHARIA ELÉTRICA e aprovada em sua forma final pelo Programa de Pós-Graduação em Engenharia Elétrica da Pontifícia Universidade Católica do Rio Grande do Sul.

DR. GUILHERME ARAUJO PIMENTEL - ORIENTADOR

BANCA EXAMINADORA

DR. JULIANO D`ORNELAS BENFICA - PROGRAMA DE PÓS-GRADUAÇÃO EM ENGENHARIA ELÉTRICA - PUCRS

DR. RICARDO RODRIGO PEREZ IBACACHE - PNPD - PUCRS

PUCRS
Av. Ipiranga, 6681 - Predio 32 - Sala 505 | CEP 90619-900 | Porto Alegre, RS - Brasil
Fone: (51) 3320-3540 | E-mail: engenharia.pg.eletrica@pucrs.br | www.pucrs.br/politecnica

Acknowledgments

First and foremost, I want to sincerely thank my supervisor Prof. Guilherme Araujo Pimentel for his invaluable guidance, patience, availability and trust in leading me to write this dissertation. I would also like to express how grateful I am to my last supervisor Aurélio Tergolina Salton for the knowledge and extensive contribution to this work.

Second, I thank my associate Emil Raymundo Bellmann and my friends for understanding my absence during my graduate study and friendship.

Finally, I would like to express my deepest gratitude to my parents, Antonio Marcos Soares Borges and Anna Deborah Werthein Serpa, my grandparents, Jorge Solidonio Serpa and Anna Maria Werthein Serpa, my deceased grandparents Antonio Chaves Borges and Maria Alice Soares Borges, who would be very proud at this moment, and all my family for their endless love, incentive and support. This work is for you.

Abstract

This work proposes a semidefinite optimization solution to the analysis and control of a torpedo shaped Autonomous Underwater Vehicle (AUV). The AUV is best described as a nonlinear system and a quaternion representation was used to represent rotations in space. The system is described by means of the Differential Algebraic Representation (DAR) which group the nonlinearities in an auxiliary vector, then a convex optimization problem subject to a set of constraint functions in the form of Linear Matrix Inequalities (LMI) ensures local exponential stability of the system attitude. A control design strategy is proposed in order to compute gain K of the closed loop system in three different scenarios in order to investigate the impact of the size of region $\mathcal{X}$ and the error of system identification at the size of region of attraction.

Keywords: Autonomous Underwater Vehicle, Torpedo, Differential Algebraic Representation, Quaternions, Linear Matrix Inequalities, Convex Optimal Problem, Semidefinite Optimization, Lyapunov Stability, Region of Attraction, Locally Exponentially Stable, Disturbance Rejection.

Resumo

Este trabalho propõe uma solução optimizada semidefinida para a análise e controle de um Veículo Subaquático Autônomo (VSA) no formado de um torpedo. O VSA é descrito por um sistema não linear e uma representação por quaternions é usada para representar rotações no espaço. O sistema é descrito em termos de uma Representação Algébrica Diferencial (RAD), a qual agrupa as não linearidades em um vetor auxiliar, então um problema de optimização convexo sujeito a um conjunto de funções de restrição na forma de Desigualdades Matriciais Linearess (DML) garante estabilidade exponencial local da orientação do sistema. Uma estratégia de controle é proposta para calcular o ganho K do sistema em malha fechada em três diferentes cenários com o objetivo de investigar o impacto do tamanho da região $\mathcal{X}$ e de possíveis erros na identificação do sistema no tamanho da região de atração.

Palavras-chave: Veículo Subaquático Autônomo, Torpedo, Representação Algébrica Diferencial, Quaternions, Desigualdades Matriciais Lineares, Problema de Optimização Convexo, Optimização Semi definida, Estabilidade de Lyapunov, Região de Atração, Estabilidade Exponencial Local, Rejeição de Distúrbios.

List of Figures

List of Tables

List of Acronyms

AUV	Autonomous Underwater Vehicle
DAR	Differential Algebraic Representation
DOA	Domain of Attraction
DOF	Degree of Freedom
LAUV	Light Autonomous Underwater Vehicle
NN	Neural Networks
ROV	Remotely Operated Vehicle
SNAME	Society of Naval Architects and Marine Engineers
USTL	Underwater Systems and Technology Laboratoty

List of Symbols

$\times$	vector cross product
$\star$	transpose of blocks outside the main diagonal block
$\|x\|$	modulus of x
$\|\|x\|\|$	euclidean norm x
$diag\{A, B\}$	block diagonal matrix composed by A and B
A^{-1}	inverse of matrix A
A'	transpose of matrix A
$\mathbb{H}$	Hamiltonian domain
$\mathbb{R}$	real domain
$\mathbb{R}^n$	real euclidean space of order n
$\mathbb{R}^{n\times m}$	real matrix space of dimension $n \times m$
$I_{n\times m}$	identity matrix of dimension $n \times m$
$O_{n\times m}$	zeros matrix of dimension $n \times m$
M_{RB}	inertia matrix of a rigid body
M_A	inertia matrix of added mass
M	inertia matrix
$C_{RB}(x)$	Coriolis and centripetal matrix of a rigid body
$C_A(x)$	Coriolis and centripetal matrix of added mass
$C(x)$	Coriolis and centripetal matrix
$D(x)$	damping effects matrix
D_l	linear damping coefficients of damping effect
D_q	quadratic damping coefficients of damping effect

$g(\boldsymbol{p}_o)$	restoring forces
W	weight force of the vehicle
B	buoyancy force of the vehicle
J	Jacobian matrix
I_{RB}	inertia matrix of the vehicle with respect to the B-frame origin
O_{RB}	origin of the body-fixed reference frame
X_{RB}	longitudinal axis (directed from aft to fore) of the body-fixed reference frame
Y_{RB}	transverse axis (directed to starboard) of the body-fixed reference frame
Z_{RB}	normal axis (directed from top to bottom) of the body-fixed reference frame
O_I	origin of the earth-fixed reference frame
X_I	longitudinal axis of the earth-fixed reference frame
Y_I	transverse axis of the earth-fixed reference frame
Z_I	normal axis of the earth-fixed reference frame
$\boldsymbol{r}_G$	center of gravity, $\boldsymbol{r}_G = [\boldsymbol{g}_x, \boldsymbol{g}_y, \boldsymbol{g}_z]'$
$\boldsymbol{g}_x, \boldsymbol{g}_y, \boldsymbol{g}_z$	components x, y, z of the center of gravity
$\boldsymbol{p}$	position vector, $\boldsymbol{p} = [\boldsymbol{p}_p, \boldsymbol{p}_o]'$
$\boldsymbol{p}_p$	linear position vector, $\boldsymbol{p}_p = [\boldsymbol{p}_x, \boldsymbol{p}_y, \boldsymbol{p}_z]'$
$\boldsymbol{p}_x, \boldsymbol{p}_y, \boldsymbol{p}_z$	linear position components in the earth-fixed frame
$\boldsymbol{p}_o$	orientation vector, $\boldsymbol{p}_o = [\boldsymbol{p}_\phi, \boldsymbol{p}_\theta, \boldsymbol{p}_\psi]'$
$\boldsymbol{p}_\phi, \boldsymbol{p}_\theta, \boldsymbol{p}_\psi$	angular position components in the earth-fixed frame
$\boldsymbol{\nu}$	velocity vector, $\boldsymbol{\nu} = [\boldsymbol{\upsilon}, \omega]'$
$\boldsymbol{\upsilon}$	linear velocity vector, $\boldsymbol{\upsilon} = [u, v, w]'$
u, v, w	linear velocity components in the body-fixed frame
ω	angular velocity vector, $\omega = [p, q, r]'$
p, q, r	angular velocity components in the body-fixed frame

$\boldsymbol{\omega}$	angular velocity vector in DAR context, $\boldsymbol{\omega} = [\boldsymbol{\omega}_1, \boldsymbol{\omega}_2, \boldsymbol{\omega}_3]'$
$\boldsymbol{\omega}_1, \boldsymbol{\omega}_2, \boldsymbol{\omega}_3$	angular velocity components in DAR context
q	quaternion in the Hamiltonian domain
$\boldsymbol{q}$	quaternion in vector form, $\boldsymbol{q} = [\eta, \epsilon]'$
η	scalar part of the quaternion
ϵ	vector part of the quaternion, $\epsilon = [\epsilon_1, \epsilon_2, \epsilon_3]'$
$\vec{r}$	unity vector around the rotation is performed
ψ	rotating angle
$\epsilon_1, \epsilon_2, \epsilon_3$	imaginary components of the quaternion
x^*	conjugate of vector x
$\dot{x}$	first derivative of x relative to time
$S(\cdot)$	skew-symmetric matrix function
$\square$	end of proof
$\blacksquare$	end of theorem and definition
$\boldsymbol{x}$	state vector
$\boldsymbol{\tau}$	torques vector applied to the vehicle
$\boldsymbol{\tau}_E$	environmental forces
u	control input vector
A_1, A_2	constant matrix of DAR
Ω_1, Ω_2	affine matrix of DAR
ξ	auxiliary vector that groups nonlinear terms of DAR
k_1, k_2, k_3	positive scalars applied to Lemma 2.1
$\mathcal{R}$	region of attraction
$\mathcal{X}$	domain of interest
K	feedback gain
P, Q_i, N	optimization variables for the LMI
L, M_i	constant matrix for the LMI

$\zeta_1, \zeta_2, \zeta_3$	auxiliary vectors
$\beta_1, \beta_2, \beta_3$	scalar functions
l	length of the vehicle
m	mass of the vehicle
d	diameter of the vehicle
$\overline{x}$	max value for x

Contents

1 Introduction

In the past few decades, the expansion of activities in deep sea growth the interest and attracted substantial attention of the control community for researching and developing technologies that help the human beings to discover and explore the submarine world. The advancement of Autonomous Underwater Vehicles (AUV) over Remotely Operated Vehicles (ROV) made a strong movement towards that due to their capability of manipulating material and collecting pertinent data at long-range, low-cost and rapid response (Silva and Sousa, 2008). Many applications may be performed by these classes of vehicles like oceanographic mapping, rescue, environmental surveying and sampling, undersea cable and structure inspection, explorations, offshore oil installations, deep sea archaeology, military interest and others (Pettersen and Egeland, 1996; Yuh, 2000). Even though marine robotic vehicles represent a very active research area, we have not been able to explore the full depths of the ocean and its abundant living and non-living resources yet, what implies that it is a considerably promising industry for working in the next several decades.

In fact, it is extremely challenging to travel undersea in consequence of the unstructured and hazardous ocean environment (Yuh et al., 2011). Some of the main researched topics for making the vehicles fully autonomous and reliable include the following subsystems and works: robust underwater communication (Chitre et al., 2008), on-board navigation sensors (Blidberg and Jalbert, 1995; Black and Butler, 1994; Paull et al., 2014), high density power sources (Hasvold et al., 2006; Bradley et al., 2001), mechanical manipulators (Shukla and Karki, 2016), pressure hulls and fairing (Walton et al., 1993; Davies and Rajapakse, 2014), fault detection and tolerance (Joshi and Talange, 2016; Podder et al., 2001; Yang et al., 1998), dynamics (Triantafyllou and Amzallag, 1984; Sagatun, 1992; Fossen et al., 1994), motion planning (Cui et al., 2016) and control systems. The last is a critical topic, since it is directly responsible for providing accurate and autonomous control, subject to environmental disturbances, uncertainties in hydrodynamic coefficients, changes in the center of gravity and buoyancy due to manipulator motions and high nonlinear, coupled and time varying dynamics of the vehicle (Yuh, 2000).

The problem of advanced underwater robot control systems has attracted many re-

searchers and several solutions have been proposed in the literature (Tsukamoto et al., 1997). A variety of methods have been designed ranging from sliding mode control, nonlinear control, adaptive control, to neural networks control and fuzzy control. The substantial quantity of publications evidence the interest of the control community in applying advanced nonlinear techniques to Autonomous Underwater Vehicles.

Yoerger and Slotine (1985) have investigated the effects of uncertainty of the hydrodynamic coefficients and negligence of cross-coupling terms and proposed a sliding mode controller for trajectory control that handle these problems effectively. Healey and Lienard (1993) have used a multivariable sliding mode autopilot based on state feedback for control underwater vehicles. Bessa et al. (2010) described the development of a dynamic positioning system for remotely operated underwater vehicles using sliding mode control strategy and enhanced by an adaptive fuzzy algorithm for uncertainty/disturbance compensation.

Nakamura and Savant (1992) presented a nonlinear tracking control that makes use of the nonholonomic nature of the system without considering the dynamics of the system.

Goheen and Jefferys (1990) have proposed two multivariable selftuning controllers as an autopilot for underwater vehicles to overcome model uncertainties. Yuh (1990a) presented an adaptive control system providing high performance in the presence of unpredictable changes in the dynamics of the vehicle and its environment. Adaptive control techniques were implemented to the design of robust controllers that can adjust to changing dynamics and operating conditions by Cristi et al. (1990). An investigation by Tabaii et al. (1994) showed an hybrid adaptive controller that handles the uncertainties dynamics. A control system is described using the bound estimation techniques, capable of learning, and adapting to changes in the vehicle dynamics and parameters by Choi and Yuh (1996). Sahu and Subudhi (2014) proposed an adaptive controller using a regressor matrix consisting hydrodynamic parameter uncertainties and the control law is verified using Lyapunov's stability criterion.

Experimental results on the application of Neural Networks (NN) to control the underwater robotic vehicle ODIN are shown by Yuh (1990b) and Lorentz and Yuh (1996). Cui et al. (2017) investigated the trajectory tracking problem using NN for compensating unknown dynamics.

A fuzzy logic controller for depth control of Unmanned Underwater Vehicles which

does not require a dynamic model was developed by DeBitetto (1995). Ishaque et al. (2010) proposed a single input single output fuzzy logic controller. Xiang et al. (2017) presented a robust fuzzy control scheme that reduces the design and implementation costs since it relaxes the knowledge of the accuracy dynamics and environmental disturbance.

In this dissertation, we will consider a dynamic model of an Autonomous Underwater Vehicle, describing Coriolis and centripetal terms, damping terms, hydrodynamic added mass and torque controls, following the notation from the Society of Naval Architects and Marine Engineers (SNAME, Lewis (1989)). The system will be expressed in terms of quaternions, then will be described in a Differential Algebraic Representation (Trofino and Dezuo, 2014). Thus, a convex optimization problem subjected to a set of constraint functions will be applied to the closed loop system in the above representation providing sufficient conditions to ensure local exponential stability of the system attitude. The proposed method do not use any kind of approximation or linearization and a collection of linear-like tools may subsequently be applied, simplifying and enriching the control design task. Finally, an investigation to the impact of disturbances in the size of the Region of Attraction will be presented. The main goals of this work are summarized in Section 1.1.

Figure 1: Light Autonomous Underwater Vehicle (LAUV) design and built at University of Porto.

Source:(Silva and Sousa, 2008).

The Autonomous Underwater Vehicle studied in this dissertation consists of a six degrees of freedom (DOF) torpedo shaped vehicle actuated by one propeller and 3 fins,

all electrically driven. The vehicle parameters were taken from an AUV optimized for small size and low-cost mechanical structure (da Silva et al., 2007) designed and built at the Underwater Systems and Technology Laboratory (USTL) from Oporto University, called Light Autonomous Underwater Vehicle (LAUV), depicted in Figure 1.

1.1 Objectives

The main aim of this work is to present an attitude control method for an Autonomous Underwater Vehicle (AUV) in the shape of torpedo such that the control design task may be cast as a semidefinite optimization problem. The following goals lead this work to the main objective

- Present the dynamics equations of the AUV in terms of quaternions
- Describe the system in the Differential Algebraic Representation
- Assess stability of the origin subjected to a proposed control law
- Compute the gain K of the closed loop system
- Investigate the impact of disturbances in the size of the Region of Attraction

In order to achieve that, the next section describes how the content of each chapter advances us towards these objectives.

1.2 Structure

This work has 6 Chapters and is organized as follows. Chapter 2 explores the main concepts and theories needed along this dissertation, especially the definition of quaternions, the application of convex optimization problems with linear matrix inequalities as constraints, depicting a system in a differential algebraic representation, the understanding of stability by Lyapunov and mathematical tools. Next, on Chapter 3, the dynamic model of a generic autonomous underwater vehicle is presented along with a specific torpedo model and its DAR form. In Chapter 4, the model is analyzed with a theorem that guarantees local exponential stability, then a design strategy is provided for the closed loop system in order to compute gain K. Going further, Chapter 5 shows the numerical results obtained from this work. Finally, in Chapter 6 the final considerations are granted and future research proposals are given.

2 Preliminaries

This chapter will lay the main concepts and the mathematical foundation used throughout this work. First, some essential mathematical tools will be briefly presented, followed by the extension of rank 4 to complex numbers, called quaternions and its application to this work. Next, the process of achieving optimal solutions, known as convex optimization problems, is presented along to the introduction to linear matrix inequalities. Finally, the concept of Lyapunov stability is discussed and a theorem is explored as constraint functions to assess exponential stability.

2.1 Mathematical Tools

Here, some mathematical tools that are necessary in the resolution of this work are presented.

Definition 2.1 (Skew-Symmetry)**.** *A matrix function* $S(x) : \mathbb{R}^3 \to \mathbb{R}^{3\times3}$ *is a skew-symmetric matrix operator defined such that the vector cross product*

$$x \times y \triangleq S(x)y \tag{1}$$

that is

$$S = -S' \tag{2}$$

and

$$S(x) = \begin{bmatrix} 0 & -x_3 & x_2 \\ x_3 & 0 & -x_1 \\ -x_2 & x_1 & 0 \end{bmatrix}, \forall x = \begin{bmatrix} x_1 \\ x_2 \\ x_3 \end{bmatrix} \in \mathbb{R}^3 \tag{3}$$

■

2.2 Quaternions

A research made by William Hamilton for a generalization of complex numbers in order to apply them to three-dimensional space resulted in 1843 in the discovery of an extension of rank 4 to complex numbers, which he named quaternions, described in a hyper-complex domain, also called Hamiltonian domain (Hamilton, 1844). Today there are many applications where they are used as for color image compression with Quaternion

Neural Networks (Isokawa et al., 2003), eletromagnetics (Anastassiu et al., 2003), and for expressing rotations and attitude of a rigid body in a three-dimensional space as described later in this section.

A quaternion, $q \in \mathbb{H}$, can be written as a sum of one real part and three imaginary parts

$$q = \eta + \epsilon_1 i + \epsilon_2 j + \epsilon_3 k \tag{4}$$

where the scalars $\eta, \epsilon_1, \epsilon_2, \epsilon_3 \in \mathbb{R}$ are the components of quaternion, while η is the scalar part and $\epsilon_1, \epsilon_2, \epsilon_3$ is the vector part. The imaginary identities i, j, k take an important role and they are the basis elements of Hamiltonian domain since they satisfy this conditions known as Hamilton's Rules

$$i^2 = j^2 = k^2 = ijk = -1. \tag{5}$$

The set of quaternions can be written as

$$\mathbb{H} = \{q = \eta + \epsilon_1 i + \epsilon_2 j + \epsilon_3 k \quad | \quad \eta, \epsilon_t \in \mathbb{R},\ \ i^2 = j^2 = k^2 = ijk = -1\}. \tag{6}$$

An alternative way of writing quaternions is the following vector form that will be used throughout the remaining chapters of this work

$$q \rightarrow \boldsymbol{q} = (\eta, \epsilon_1, \epsilon_2, \epsilon_3) = \begin{bmatrix} \eta \\ \epsilon \end{bmatrix}. \tag{7}$$

The conjugate $\boldsymbol{q}^*$ is defined as

$$q^* = \eta - \epsilon_1 i - \epsilon_2 j - \epsilon_3 k \rightarrow \boldsymbol{q}^* = \begin{bmatrix} \eta \\ -\epsilon \end{bmatrix}. \tag{8}$$

The length of $\boldsymbol{q}$ is defined as the norm

$$\|q\| = \sqrt{qq^*} \rightarrow \|\boldsymbol{q}\| = \sqrt{\boldsymbol{q}'\boldsymbol{q}} = \sqrt{\eta^2 + \epsilon_1^2 + \epsilon_2^2 + \epsilon_3^2}. \tag{9}$$

This work uses quaternions to represent rotations in a three-dimensional space. Although, Euler Angles sequences are a traditional way to represent rotations by a set of three angles and they have easy understanding, unit quaternion is a four-dimensional parametrization of attitude that provides important advantages, as smooth rotation for

rigid bodies and avoid singularities (*Gimbal Lock*) (Diebel, 2006).

From the Euler's theorem, it is known that the attitude of a rigid body can be described in terms of rotation by some angle ψ along an axis $\vec{r}$. In terms of the axis-angle rotation, quaternions are defined as

$$\boldsymbol{q} = \begin{bmatrix} \cos\frac{\psi}{2} \\ \vec{r}\sin\frac{\psi}{2} \end{bmatrix} = \begin{bmatrix} \eta \\ \epsilon \end{bmatrix} \in \mathbb{R}^4 \tag{10}$$

where $\eta \in \mathbb{R}$ is its scalar part and $\epsilon \in \mathbb{R}^3$ is its vector part. The unit vector $\vec{r} \in \mathbb{R}^3$ describes the direction around which the rotation ψ is performed, as depict in Figure 2.

Figure 2: Representation of axis-angle rotation.

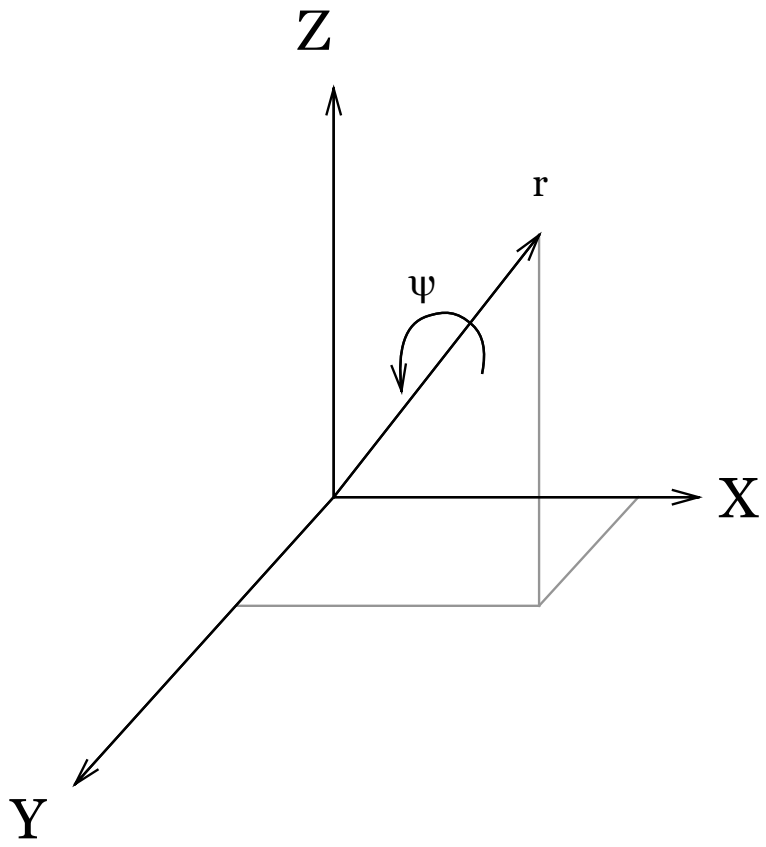

Source: the autor (2018).

Note that unit quaternions are quaternions with unity norm for natural rotations without scaling. Then it is clear that the following normalization equation is satisfied

$$\eta^2 + \epsilon'\epsilon = 1. \tag{11}$$

2.3 Convex sets

Among nonlinear functions, the convex one are the most similar to the linear. A set $C \in \mathbb{R}^n$ is said to be *convex* if either $C = 0$ or if the line connecting any two points in C is entirely contained in C (Boyd and Vandenberghe, 2004). This is said by the following

$$\delta x_1 + (1 - \delta)x_2 \in C \qquad \forall \delta \in [0, 1], \forall x_1, x_2 \in C. \tag{12}$$

Figure 3 depicts two simple sets where (a) is a nonconvex set because there are pairs of points which the segments connecting the two points cross the outside border of the set and in contrast (b) is a convex set by the opposite.

Figure 3: Two sets that easily show the definition of a convex set: (a) Nonconvex set and (b) Convex set.

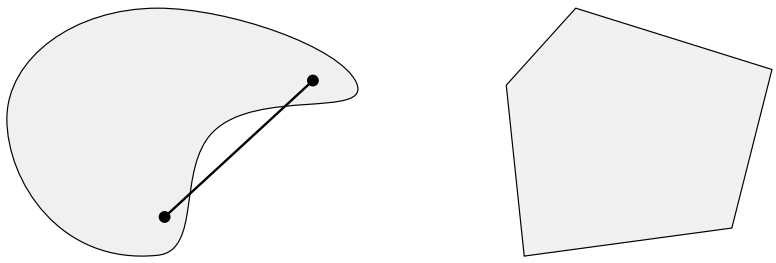

(a) (b)

Source: the author (2018).

2.4 Optimization Problems

Optimization problems are processes of choosing the best selection from a number of options or a set of candidate options (Scherer and Weiland, 2004). They are commonly found in daily life and have many examples in areas extending from sciences as engineering, automation, control, architecture and economics to biological and ecological processes and organizational questions. For example, relevant economical profits on the production of a product may only be realized if proper decisions is made in its manufacturing process.

Matching strict specifications and quality standards, with minimal waste of resources, energy and time, whereas delivering maximal economical profits are constantly demanding further optimization, for increased efficiency and a better control of processes.

A convex optimization problem is one of the form

$$\begin{aligned} &\underset{\boldsymbol{x}}{\text{minimize}} && f_0(\boldsymbol{x}) \\ &\text{subject to} && f_i(\boldsymbol{x}) \leq b_i,\ i = 1, \ldots, m. \end{aligned} \tag{13}$$

where the vector $\boldsymbol{x} = (\boldsymbol{x}_1, ..., \boldsymbol{x}_n)$ is the choice made (*optimization variable*), the function $f_0 : \mathbb{R}^n \to \mathbb{R}$ represents the cost of choosing it (*objective function*), the inequalities $f_i : \mathbb{R}^n \to \mathbb{R}$ are the requirements that limit the possible choices (*constraint functions*) and the constants $b_i, ..., b_m$ are the bounds for the constraints (Boyd and Vandenberghe, 2004).

The objective and constraint functions are convex, *i.e.*, satisfy

$$f_i(\alpha\boldsymbol{x} + \beta\boldsymbol{y}) \leq \alpha f_i(\boldsymbol{x}) + \beta f_i(\boldsymbol{y}) \tag{14}$$

for all $\boldsymbol{x}, \boldsymbol{y} \in \mathbb{R}^n$, and all $\alpha, \beta \in \mathbb{R}$ with $\alpha + \beta = 1$, $\alpha \geq 0$, $\beta \geq 0$.

A point $\boldsymbol{x}$ is feasible if it satisfies all the constraint functions. Therefore, the convex optimization problem (13) is feasible if there is at least one feasible point and its solution is represented by the point that has minimum cost among the set of all choices that meet the specifications (*feasible set*). Typically, the solving methods for this problem have no analytical formula. However, there are very effective methods based on algorithms that compute a mathematical solution for that particular problem given its properties. An example of these methods is the Interior-point methods discussed in chapter 11 of (Boyd and Vandenberghe, 2004).

In this work, we make use of a semidefinite optimization problem in the form of (13) presented on Chapter 4 to solve the task of maximization of the estimate of the region of attraction $\mathcal{R}_a$.

2.5 Differential Algebraic Representation

Consider the following uncertain nonlinear system

$$\dot{\boldsymbol{x}} = f(\boldsymbol{x}, \boldsymbol{\tau}) \tag{15}$$

where $\boldsymbol{x} \in \mathcal{X}$ denotes the state, $\boldsymbol{\tau} \in \mathcal{T}$ denotes the vector of algebraic variables and $f(\boldsymbol{x}, \boldsymbol{\tau})$ is a nonlinear vector function of $(\boldsymbol{x}, \boldsymbol{\tau})$.

The Differential Algebraic Representation (DAR) originally proposed by (Trofino, 2000) groups nonlinear terms of degree equal or higher than two in an auxiliary vector $\xi(\boldsymbol{x}, \boldsymbol{\tau})$ in order to represent rational systems. By making use of this vector, consider that system (15) can be represented in the following form

$$\dot{\boldsymbol{x}} = A_1 \boldsymbol{x} + A_2 \xi(\boldsymbol{x}, \boldsymbol{\tau}) \tag{16}$$

$$0 = \Omega_1(\boldsymbol{x}, \boldsymbol{\tau})\boldsymbol{x} + \Omega_2(\boldsymbol{x}, \boldsymbol{\tau})\xi(\boldsymbol{x}, \boldsymbol{\tau}) \tag{17}$$

where $A_1 \in \mathbb{R}^{n \times n}$ and $A_2 \in \mathbb{R}^{n \times m}$ are constant matrices, $\Omega_1(\boldsymbol{x}, \boldsymbol{\tau}) \in \mathbb{R}^{q \times n}$ and $\Omega_2(\boldsymbol{x}, \boldsymbol{\tau}) \in \mathbb{R}^{q \times m}$ are affine matrix functions of $(\boldsymbol{x}, \boldsymbol{\tau})$ and $\xi(\boldsymbol{x}, \boldsymbol{\tau}) \in \mathbb{R}^m$ is the auxiliary vector.

This representation has no unique solution being not able to compute it in a systematic way. As consequence, different estimates of the domain of attraction might be lead by different choices of A_1, A_2, $\Omega_1(\boldsymbol{x}, \boldsymbol{\tau})$, $\Omega_2(\boldsymbol{x}, \boldsymbol{\tau})$ and $\xi(\boldsymbol{x}, \boldsymbol{\tau})$.

The auxiliary variable $\xi(\boldsymbol{x}, \boldsymbol{\tau})$ may be eliminated from (16) recovering the original system representation by defining

$$\xi = -(\Omega_2' \Omega_2)^{-1} \Omega_2' \Omega_1 \boldsymbol{x} \tag{18}$$

Here, the notation was simplified by not representing the dependence of Ω_1, Ω_2 and ξ on $(\boldsymbol{x}, \boldsymbol{\tau})$.

Then, the dynamics of system (15) can be readily recovered by

$$\dot{x} = (A_1 - A_2 \Omega_2^{-1} \Omega_1)\boldsymbol{x} \tag{19}$$

2.6 Linear Matrix Inequalities in Control

The design of a controller in general has four requirements: closed-loop stability, stay stable despite model uncertainty and disturbances (*robustness*), achieve control requirements (*performance*) and remain stable and well performing despite model uncertainty and disturbances (*robust performance*). In control theory, these requirements are usually best satisfied in the form of convex optimization problems, Section 2.4, and theirs constraints stated in terms of Linear Matrix Inequalities (LMIs) (Turner and Bates, 2007).

The applicability of LMIs ranges from stability and performance evaluations, control law synthesis, optimal system realization and for many optimization problems. Even though, the concept of a LMI was first introduced in about 1890, in the work of Lyapunov, it got in prominence in the late 1980's with the development of computational algorithms (Boyd et al., 1994).

An important understanding of matrix inequalities is definiteness as follows.

Definition 2.2 (Definiteness of Matrices)**.** *Let $P \in \mathbb{R}^{n\times n}$ be a symmetric matrix. It is said to be*

a) ***Positive definite*** *if $P > 0$ and $u'Pu > 0\ \forall u \neq 0 \in \mathbb{R}^n$ (all eigenvalues are positive)*

b) ***Positive semidefinite*** *if $P \geq 0$ and $u'Pu \geq 0\ \forall u \in \mathbb{R}^n$ (all eigenvalues are nonnegative)*

c) ***Negative definite*** *if $P < 0$ and $u'Pu < 0\ \forall u \neq 0 \in \mathbb{R}^n$ (all eigenvalues are negative)*

d) ***Negative semidefinite*** *if $P \leq 0$ and $u'Pu \leq 0\ \forall u \in \mathbb{R}^n$ (all eigenvalues are nonpositive)*

The basic structure of a linear matrix inequality (LMI) has the form

$$F(\boldsymbol{x}) = F_0 + \sum_{i=1}^{m} \boldsymbol{x}_i F_i > 0 \tag{20}$$

where $F(\boldsymbol{x})$ is a definite positive matrix, which leading principal minors must be positive, $\boldsymbol{x} \in \mathbb{R}^m$ is the variable vector and $F_i = F_i' \in \mathbb{R}^{n\times n}$, $i = 0, ..., m$ are given constant symmetry matrices (Scherer and Weiland, 2004). The feasibility problem is to find $\boldsymbol{x}$ such that inequality (20) holds.

In general, its common to face systems of linear matrix inequalities. The next definition express how we can represent a set of LMIs as a single LMI.

Definition 2.3 (Multiple LMIs)**.** *Multiple Linear Matrix Inequalities is a finite set of linear matrix inequalities*

$$F_1(\boldsymbol{x}) > 0, ..., F_p(\boldsymbol{x}) > 0 \tag{21}$$

This system of LMIs can always be converted to a single LMI constraint, when disposing them diagonally

$$F(\boldsymbol{x}) = \begin{bmatrix} F_1(\boldsymbol{x}) & 0 & \dots & 0 \\ 0 & F_2(\boldsymbol{x}) & \dots & 0 \\ \vdots & & \ddots & \vdots \\ 0 & 0 & \dots & F_p(\boldsymbol{x}) \end{bmatrix} > 0. \tag{22}$$

2.6.1 Schur Complement

Even though, there are plenty of control problems that can be cast as LMI problems, a substantial number of pertinent cases have nonlinearities in its nature. In this regard, there are tools as the Schur complement that manipulates these problems in order to transform them into a suitable LMI format. In this case, it transforms quadratic matrix inequalities into linear matrix inequalities.

Considering matrix $S \in \mathbb{R}^{n\times m}$ and symmetric matrices $Q = Q' \in \mathbb{R}^{n\times n}$, $N = N' \in \mathbb{R}^{m\times m}$ with $N > 0$, the basic idea is that

$$\begin{bmatrix} Q & S \\ \star & R \end{bmatrix} > 0 \tag{23}$$

is equivalent to

$$Q - SR^{-1}S' > 0. \tag{24}$$

2.6.2 S-Procedure

In control problems, there are instances where one needs to combine several quadratic inequalities into one single inequality. The S-Procedure is a method that enables this approach.

Let symmetric matrices $A = A' \in \mathbb{R}^{n\times n}$, $B = B' \in \mathbb{R}^{n\times n}$ and assume that the quadratic inequalities are consequence of each other

$$\boldsymbol{x}'A\boldsymbol{x} \geq 0 \implies \boldsymbol{x}'B\boldsymbol{x} \geq 0 \tag{25}$$

if and only if there exists a nonnegative λ such that

$$B > \lambda A. \tag{26}$$

One of the simplest linear matrix inequality arose in control theory is the Lyapunov inequality. The following section presents a set of LMIs that are required to assess stability in the sense of Lyapunov.

2.7 Lyapunov Stability Theory

Lyapunov stability theory is a classic approach in systems theory that allows one to draw conceptual conclusions about the trajectories of a system and determine the stability without explicitly integrating the differential equations of the system (Murray, 2017). The direct method of Lyapunov makes use of an auxiliary function $V(\boldsymbol{x})$, called candidate Lyapunov function, and the concept of energy in order to give sufficient conditions that prove the stability.

Let $V(\boldsymbol{x})$ be a candidate Lyapunov function and $\dot{V}(\boldsymbol{x})$ be its derivative along trajectories of this system. If $\dot{V}(\boldsymbol{x})$ is negative throughout the region, it implies that the energy is decreasing over time. It means that a trajectory starting in a $\mathcal{R}$ neighborhood of the origin will never leave the neighborhood.

The following lemma presents the set of linear matrix inequalities required to assess exponential stability (Khalil, 1996) of a function, as Definition (2.4), that will be applied later on this work.

Definition 2.4 (Definiteness of Functions)**.** *Consider a continuously differentiable function* $V(\boldsymbol{x}), V : \mathcal{R} \mapsto \mathbb{R}$

a) Positive definite *if* $V(0) = 0$ *and* $V(\boldsymbol{x}) > 0 \ \forall \boldsymbol{x} \neq 0 \in \mathcal{X}$

b) Positive semidefinite *if* $V(0) = 0$ *and* $V(\boldsymbol{x}) \geq 0 \ \forall \boldsymbol{x} \neq 0 \in \mathcal{X}$

c) Negative definite *if* $V(0) = 0$ *and* $V(\boldsymbol{x}) < 0 \ \forall \boldsymbol{x} \neq 0 \in \mathcal{X}$

d) Negative semidefinite *if* $V(0) = 0$ *and* $V(\boldsymbol{x}) \leq 0 \ \forall \boldsymbol{x} \neq 0 \in \mathcal{X}$

Lemma 2.1. *Consider the nonlinear continuous-time autonomous system*

$$\dot{\boldsymbol{x}} = f(\boldsymbol{x}), \tag{27}$$

where $\boldsymbol{x} \in \mathcal{X}$ *is the state vector and the function* $f : \mathcal{X} \mapsto \mathbb{R}^n$ *is locally Lipschitz on* $\boldsymbol{x}$ *with equilibrium point* $\boldsymbol{x}_{eq} = 0$*. Let* $V(\boldsymbol{x}) = \boldsymbol{x}'P\boldsymbol{x}$ *be a candidate Lyapunov function such that the following is satisfied for all* $\boldsymbol{x} \in \mathcal{X}$*:*

$$k_1\boldsymbol{x}'\boldsymbol{x} \leq V(\boldsymbol{x}) \leq k_2\boldsymbol{x}'\boldsymbol{x}, \tag{28}$$

$$\dot{V}(\boldsymbol{x}) = \dot{\boldsymbol{x}}'P\boldsymbol{x} + \boldsymbol{x}'P\boldsymbol{x} \leq -k_3\boldsymbol{x}'\boldsymbol{x}, \tag{29}$$

$$\mathcal{R} := \{\boldsymbol{x} : V(\boldsymbol{x}) \leq 1\} \subset \mathcal{X}, \tag{30}$$

for positive scalars, k_1*,* k_2 *and* k_3*. Then, every trajectory starting in* $\mathcal{R}$ *exponentially approaches the origin.*

□

3 Dynamic Model

This chapter presents the most commonly used mathematical descriptions of the Autonomous Underwater Vehicle that are necessary in order to design the control method proposed in Chapter 4. For detailed description, see (Fossen et al., 1994). This chapter is organized as follows. First, the coordinate frames are briefly introduced, followed by main components that constitute the motion of marine vehicles. Next, the kinematic model is addressed presenting the geometric relationship between the body-fixed and earth-fixed frames. Then, dynamic equations of motion are described in quaternion terms using the Newton-Euler formulation. Afterwards, the external forces and moments are represented in terms of Hydrodynamic forces, Environmental forces and Propulsion forces. Finally, the system dynamic equations are simplified, illustrating the case of study.

3.1 Coordinate Frames

Consider the Autonomous Underwater Vehicle from Figure 4. When analyzing the motion of this vehicle in 6 DOF, there are two coordinate frames that are commonly used to describe the kinematics: a global inertia reference frame fixed to the Earth (I-frame) and a moving coordinate frame, fixed to the vehicle, called body-fixed reference frame (B-frame).

The local coordinate frame, (B-frame), has its origin O_{RB} chosen to coincide with the center of mass of the vehicle's body. The body axes X_{RB}, Y_{RB} and Z_{RB} coincide with the principal axes of inertia of the vehicle and are defined as

- X_{RB} - longitudinal axis (directed from aft to fore)
- Y_{RB} - transverse axis (directed to starboard)
- Z_{RB} - normal axis (directed from top to bottom)

3.2 Motion Components

The motion of marine vehicles are usually defined in six different components as shown in Table 2. The position ($\boldsymbol{p}_p$) and orientation ($\boldsymbol{p}_o$) of the vehicle are described relative to the I-frame , while the linear ($\boldsymbol{v}$) and angular (ω) velocities and the control forces

Figure 4: Body-fixed and earth-fixed reference frames.

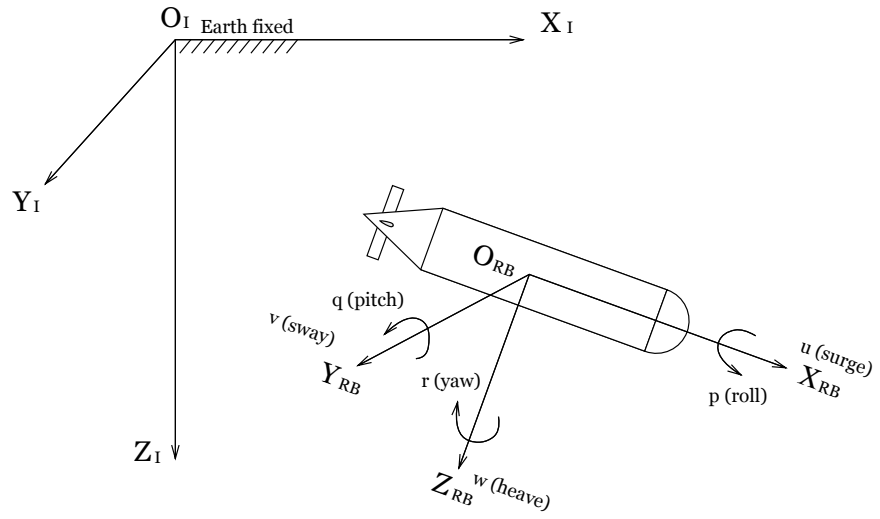

Source: the autor (2018).

($\boldsymbol{\tau}_1$) and moments ($\boldsymbol{\tau}_2$) are described in the B-frame . They are detailed in the following vectors

Table 2: Notation used for marine vehicles.

Motion component	Forces and Moments	Linear and Angular Vel.	Positions and Euler Angles
Motions in the x-direction (surge)	X	u	x
Motions in the y-direction (sway)	Y	v	y
Motions in the z-direction (heave)	Z	w	z
Rotation about the x-axis (roll)	K	p	ϕ
Rotation about the y-axis (pitch)	M	q	θ
Rotation about the z-axis (yaw)	N	r	ψ

Source: adapted from Fossen et al. (1994)

$$\boldsymbol{p} = \begin{bmatrix} \boldsymbol{p}_p \\ \boldsymbol{p}_o \end{bmatrix} = \begin{bmatrix} \boldsymbol{p}_x & \boldsymbol{p}_y & \boldsymbol{p}_z & \boldsymbol{p}_\phi & \boldsymbol{p}_\theta & \boldsymbol{p}_\psi \end{bmatrix}' \in \mathbb{R}^6 \tag{31}$$

$$\boldsymbol{\nu} = \begin{bmatrix} \boldsymbol{v} \\ \omega \end{bmatrix} = \begin{bmatrix} u & v & w & p & q & r \end{bmatrix}' \in \mathbb{R}^6 \tag{32}$$

$$\boldsymbol{\tau} = \begin{bmatrix} \boldsymbol{\tau}_1 \\ \boldsymbol{\tau}_2 \end{bmatrix} = \begin{bmatrix} X & Y & Z & K & M & N \end{bmatrix}' \in \mathbb{R}^6 \tag{33}$$

3.3 Quaternion-based Kinematic Model

The geometric relationship between the earth-fixed and the vehicle-fixed motions is described by the kinematic model (Fossen et al., 1994). The body-fixed reference frame and the inertial reference frame are related through a transformation matrix $J(\boldsymbol{q})$ according to

$$\begin{bmatrix} \dot{\boldsymbol{p}} \\ \dot{\boldsymbol{q}} \end{bmatrix} = \begin{bmatrix} J_1(\boldsymbol{q}) & 0_{3\times 3} \\ 0_{4\times 3} & \frac{1}{2}J_2(\boldsymbol{q}) \end{bmatrix} \begin{bmatrix} \boldsymbol{v} \\ \omega \end{bmatrix} \Longleftrightarrow \dot{\xi} = J(\boldsymbol{q})\boldsymbol{\nu} \in \mathbb{R}^7 \tag{34}$$

where $\boldsymbol{p} = [\boldsymbol{p}_x, \boldsymbol{p}_y, \boldsymbol{p}_z]' \in \mathbb{R}^3$ is the I-frame position vector of the vehicle, $\boldsymbol{q} = [\eta, \epsilon']' = [\eta, \epsilon_1, \epsilon_2, \epsilon_3]'$ is the unit quaternion representing the body attitude (with scalar and vector parts $\eta \in \mathbb{R}$ and $\epsilon \in \mathbb{R}^3$, respectively), $\boldsymbol{v} = [u, v, w]' \in \mathbb{R}^3$ and $\omega = [p, q, r]' \in \mathbb{R}^3$ are the linear and angular velocities of the vehicle in the B-frame .

The rotation matrix $J_1(\boldsymbol{q}) \in \mathbb{R}^{3\times 3}$ that relates the linear velocity vector in the I-frame to the velocity in the B-frame can be expressed as

$$J_1(\boldsymbol{q}) = \begin{bmatrix} 1-2(\epsilon_2^2+\epsilon_3^2) & 2(\epsilon_1\epsilon_2-\epsilon_3\eta) & 2(\epsilon_1\epsilon_3+\epsilon_2\eta) \\ 2(\epsilon_1\epsilon_2+\epsilon_3\eta) & 1-2(\epsilon_1^2+\epsilon_3^2) & 2(\epsilon_2\epsilon_3-\epsilon_1\eta) \\ 2(\epsilon_1\epsilon_3-\epsilon_2\eta) & 2(\epsilon_2\epsilon_3+\epsilon_1\eta) & 1-2(\epsilon_1^2+\epsilon_2^2) \end{bmatrix} \tag{35}$$

The coordinate transformation matrix $J_2(\boldsymbol{q}) \in \mathbb{R}^{4\times 3}$ that relates the angular velocity vector in the I-frame to the velocity in the B-frame can be expressed as

$$J_2(\boldsymbol{q}) = \begin{bmatrix} -\epsilon' \\ \eta I_{3\times 3} + S(\epsilon) \end{bmatrix} \tag{36}$$

where $I_{3\times 3}$ is the 3×3 identity matrix and $S(\cdot)$ is a skew-symmetric matrix.

3.4 Dynamics of Autonomous Underwater Vehicles

The dynamics of Autonomous Underwater Vehicles with 6 Degrees of Freedom can be represented in the B-frame by the nonlinear equation

$$M\dot{\boldsymbol{\nu}} + C(\boldsymbol{\nu})\boldsymbol{\nu} + D(\boldsymbol{\nu})\boldsymbol{\nu} + g(\boldsymbol{p}_o) = \boldsymbol{\tau} + \boldsymbol{\tau}_E \tag{37}$$

where M is the total inertial matrix that includes rigid-body and added mass, $C(\boldsymbol{\nu})$ is the total Coriolis and centripetal terms of the rigid-body and added mass, $D(\boldsymbol{\nu})$ is the total hydrodynamic damping matrix, $g(\eta)$ is the gravitational and buoyant forces, $\boldsymbol{\tau}$ is the propulsion forces (control input) and $\boldsymbol{\tau}_E$ is the environmental forces.

The total inertial matrix is defined by

$$M = M_{RB} + M_A \tag{38}$$

The total Coriolis and centripetal matrix is defined by

$$C(\boldsymbol{\nu}) = C_{RB}(\boldsymbol{\nu}) + C_A(\boldsymbol{\nu}) \tag{39}$$

The total hydrodynamic damping matrix is defined by

$$D(\boldsymbol{\nu}) = D_P(\boldsymbol{\nu}) + D_S(\boldsymbol{\nu}) + D_W(\boldsymbol{\nu}) + D_M(\boldsymbol{\nu}) \tag{40}$$

The following sections will approach each term of Equation (37) individually.

3.4.1 Rigid-body Dynamics

The nonlinear dynamic equations of Rigid-body Vehicles are given by

$$M_{RB}\dot{\boldsymbol{\nu}} + C_{RB}(\boldsymbol{\nu})\boldsymbol{\nu} = \boldsymbol{\tau}_{RB} \tag{41}$$

where $M_{RB} \in \mathbb{R}^{6\times6}$ is the rigid-body inertial matrix, $C_{RB}(\boldsymbol{\nu}) \in \mathbb{R}^{6\times6}$ is the rigid-body Coriolis and centripetal matrix and $\boldsymbol{\tau}_{RB} = [\boldsymbol{\tau}_1', \boldsymbol{\tau}_2']' = [X, Y, Z, K, M, N]' \in \mathbb{R}^6$ is a generalized vector of external forces and moments.

The rigid-body inertial matrix is defined by

$$M_{RB} = \begin{bmatrix} mI_{3\times 3} & -mS(\boldsymbol{r}_G) \\ mS(\boldsymbol{r}_G) & I_{RB} \end{bmatrix} = \begin{bmatrix} m & 0 & 0 & 0 & m\boldsymbol{g}_z & -m\boldsymbol{g}_y \\ 0 & m & 0 & -m\boldsymbol{g}_z & 0 & m\boldsymbol{g}_x \\ 0 & 0 & m & m\boldsymbol{g}_y & -m\boldsymbol{g}_x & 0 \\ 0 & -m\boldsymbol{g}_z & m\boldsymbol{g}_y & I_x & -I_{xy} & -I_{xz} \\ m\boldsymbol{g}_z & 0 & -m\boldsymbol{g}_x & -I_{yx} & I_y & -I_{yz} \\ -m\boldsymbol{g}_y & m\boldsymbol{g}_x & 0 & -I_{zx} & -I_{zy} & I_z \end{bmatrix} \tag{42}$$

where m is the constant mass, $I_{3\times 3}$ is the identity matrix, $\boldsymbol{r}_G = [\boldsymbol{g}_x, \boldsymbol{g}_y, \boldsymbol{g}_z]'$ is the center of gravity, $I_{RB} = I'_{RB} > 0$ is the inertia tensor with respect to O_{RB} and $S(\cdot) \in SS(3)$ is defined in Definition 2.1.

The inertia tensor matrix of the rigid-body is

$$I_{RB} = \begin{bmatrix} I_x & -I_{xy} & -I_{xz} \\ -I_{yx} & I_y & -I_{yz} \\ -I_{zx} & -I_{zy} & I_z \end{bmatrix} \tag{43}$$

where I_x, I_y and I_z are moments of inertia about the X_{RB}, Y_{RB} and Z_{RB}-axes.

The rigid-body Coriolis and centripetal matrix is defined by

$$C_{RB}(\boldsymbol{\nu}) = \begin{bmatrix} 0_{3\times 3} & -mS(\boldsymbol{v}) - mS(\omega)S(\boldsymbol{r}_G) \\ -mS(\boldsymbol{v}) + mS(\boldsymbol{r}_G)S(\omega) & -S(I_{RB}\omega) \end{bmatrix}, \tag{44}$$

which is represented by

$$C_{RB}(\boldsymbol{\nu}) = \begin{bmatrix} 0 & 0 & 0 \\ 0 & 0 & 0 \\ 0 & 0 & 0 \\ -m(\boldsymbol{g}_y q + \boldsymbol{g}_z r) & m(\boldsymbol{g}_y p + w) & m(\boldsymbol{g}_z p - v) \\ m(\boldsymbol{g}_x q - w) & -m(\boldsymbol{g}_z r + \boldsymbol{g}_x p) & m(\boldsymbol{g}_z q + w) \\ m(\boldsymbol{g}_x r + v) & m(\boldsymbol{g}_y r - u) & -m(\boldsymbol{g}_x p + \boldsymbol{g}_y q) \end{bmatrix} \begin{bmatrix} m(\boldsymbol{g}_y q + \boldsymbol{g}_z r) & -m(\boldsymbol{g}_x q - w) & -m(\boldsymbol{g}_x r + v) \\ -m(\boldsymbol{g}_y p + w) & m(\boldsymbol{g}_z r + \boldsymbol{g}_x p) & -m(\boldsymbol{g}_y r - u) \\ -m(\boldsymbol{g}_z p - v) & -m(\boldsymbol{g}_z q + u) & m(\boldsymbol{g}_x p + \boldsymbol{g}_y q) \\ 0 & -I_{yz} q - I_{xz} p + I_z r & I_{yz} r + I_{xy} p - I_y q \\ I_{yz} q + I_{xz} p - I_z r & 0 & -I_{xz} r - I_{xy} q + I_x p \\ -I_{yz} r - I_{xy} p + I_y q & I_{xz} r + I_{xy} q - I_x p & 0 \end{bmatrix} \tag{45}$$

This structure used for control design is a compact form of

$$m(\dot{\boldsymbol{\upsilon}} + \omega \times \boldsymbol{\upsilon} + \dot{\omega} \times \boldsymbol{r}_G + \omega \times (\omega \times \boldsymbol{r}_G)) = \boldsymbol{\tau}_1 \tag{46}$$

$$I_{RB}\dot{\omega} + \omega \times (I_{RB}\omega) + m\boldsymbol{r}_G \times (\dot{\boldsymbol{\upsilon}} + \omega \times \boldsymbol{\upsilon}) = \boldsymbol{\tau}_2 \tag{47}$$

where $\boldsymbol{\tau}_{RB} = [\boldsymbol{\tau}_1', \boldsymbol{\tau}_2']' = [X, Y, Z, K, M, N]' \in \mathbb{R}^6$ is a generalized vector of external applied forces and moments, respectively.

3.4.2 External Forces and Moments

The right-hand side vector term $\boldsymbol{\tau}_{RB}$ of Equation (41) represents the external forces and moments acting on the vehicle. These external forces and moments can be represented in terms of *Hydrodynamic forces*, *Environmental forces* and *Propulsion forces*, as expressed in the following equation

$$\boldsymbol{\tau}_{RB} = \boldsymbol{\tau}_H + \boldsymbol{\tau}_E + \boldsymbol{\tau} \tag{48}$$

where $\boldsymbol{\tau}_H$, $\boldsymbol{\tau}_E$ and $\boldsymbol{\tau}$ are the Hydrodynamic forces, Environmental forces and Propulsion forces, respectively.

3.4.2.1 Hydrodynamic Forces and Moments Hydrodynamic forces and moments are composed by the sum of two components as

$$\boldsymbol{\tau}_H = \boldsymbol{\tau}_R + \boldsymbol{\tau}_D \tag{49}$$

where $\boldsymbol{\tau}_R$ is the radiation-induced forces and $\boldsymbol{\tau}_D$ is the damping effects.

Radiation-induced forces are forces that act on the body when it is forced to oscillate with the wave excitation frequency and there are no incident waves. The radiation-induced forces can be defined as the sum of three new components

$$\boldsymbol{\tau}_R = -M_A\dot{\boldsymbol{\nu}} - C_A(\boldsymbol{\nu})\boldsymbol{\nu} - D_P(\boldsymbol{\nu})\boldsymbol{\nu} - g(\boldsymbol{p}_o) \tag{50}$$

where $-M_A\dot{\boldsymbol{\nu}} - C_A(\boldsymbol{\nu})\boldsymbol{\nu}$ is the added mass, $-D_P(\boldsymbol{\nu})\boldsymbol{\nu}$ is the potential damping and $g(\eta)$ is the restoring forces.

Added mass can be understood as pressure-induced forces and moments due to a forced harmonic motion of the body which are proportional to the acceleration of the body. The added inertia matrix M_A is defined as

$$M_A = \begin{bmatrix} A_{11} & A_{12} \\ A_{21} & A_{21} \end{bmatrix} = - \begin{bmatrix} X_{\dot{u}} & X_{\dot{v}} & X_{\dot{w}} & X_{\dot{p}} & X_{\dot{q}} & X_{\dot{r}} \\ Y_{\dot{u}} & Y_{\dot{v}} & Y_{\dot{w}} & Y_{\dot{p}} & Y_{\dot{q}} & Y_{\dot{r}} \\ Z_{\dot{u}} & Z_{\dot{v}} & Z_{\dot{w}} & Z_{\dot{p}} & Z_{\dot{q}} & Z_{\dot{r}} \\ K_{\dot{u}} & K_{\dot{v}} & K_{\dot{w}} & K_{\dot{p}} & K_{\dot{q}} & K_{\dot{r}} \\ M_{\dot{u}} & M_{\dot{v}} & M_{\dot{w}} & M_{\dot{p}} & M_{\dot{q}} & M_{\dot{r}} \\ N_{\dot{u}} & N_{\dot{v}} & N_{\dot{w}} & N_{\dot{p}} & N_{\dot{q}} & N_{\dot{r}} \end{bmatrix} \tag{51}$$

where the element A_{ij} of added mass force along the i^{th}-axis due to an acceleration in the j^{th} direction as example

$$M_{12} = X_{\dot{v}} \tag{52}$$

The matrix of hydrodynamic Coriolis and centripetal terms is defined as

$$C_A(\boldsymbol{\nu}) = \begin{bmatrix} 0_{3\times3} & -S(A_{11}\boldsymbol{\upsilon} + A_{12}\omega) \\ -S(A_{11}\boldsymbol{\upsilon} + A_{12}\omega) & -S(A_{21}\boldsymbol{\upsilon} + A_{22}\omega) \end{bmatrix} \tag{53}$$

Considering that motions of submarine vehicles at high speed are highly nonlinear and

coupled, there are some considerations that can be done in order to simplify the model. It is important to highlight that the torpedo vehicle studied in this work, as in many other submarine applications, will move at low speed. Notice that due to vehicle symmetries, some coefficients that affect the motion can be neglected. If we consider three planes of symmetry, all elements from the off-diagonal would be neglected. Hence, the following simple expressions for M_A and C_A are obtained

$$M_A = -\begin{bmatrix} X_{\dot{u}} & 0 & 0 & 0 & 0 & 0 \\ 0 & Y_{\dot{v}} & 0 & 0 & 0 & 0 \\ 0 & 0 & Z_{\dot{w}} & 0 & 0 & 0 \\ 0 & 0 & 0 & K_{\dot{p}} & 0 & 0 \\ 0 & 0 & 0 & 0 & M_{\dot{q}} & 0 \\ 0 & 0 & 0 & 0 & 0 & N_{\dot{r}} \end{bmatrix} \tag{54}$$

$$C_A(\boldsymbol{\nu}) = \begin{bmatrix} 0 & 0 & 0 & 0 & -Z_{\dot{w}}w & Y_{\dot{v}}v \\ 0 & 0 & 0 & Z_{\dot{w}}w & 0 & -X_{\dot{u}}u \\ 0 & 0 & 0 & -Y_{\dot{v}}v & X_{\dot{u}}u & 0 \\ 0 & -Z_{\dot{w}}w & Y_{\dot{v}}v & 0 & -N_{\dot{r}}r & M_{\dot{q}}q \\ Z_{\dot{w}}w & 0 & -X_{\dot{u}}u & N_{\dot{r}}r & 0 & -K_{\dot{p}}p \\ -Y_{\dot{v}}v & X_{\dot{u}}u & 0 & -M_{\dot{q}}q & K_{\dot{p}}p & 0 \end{bmatrix} \tag{55}$$

Given the above, the total inertial matrix (38) is defined by the sum of (42) to (51)

$$M = \begin{bmatrix} m - X_{\dot{u}} & -X_{\dot{v}} & -X_{\dot{w}} & -X_{\dot{p}} & m\boldsymbol{g}_z - X_{\dot{q}} & -m\boldsymbol{g}_y - X_{\dot{r}} \\ -Y_{\dot{u}} & m - Y_{\dot{v}} & -Y_{\dot{w}} & -m\boldsymbol{g}_z - Y_{\dot{p}} & -Y_{\dot{q}} & m\boldsymbol{g}_x - Y_{\dot{r}} \\ -Z_{\dot{u}} & -Z_{\dot{v}} & m - Z_{\dot{w}} & m\boldsymbol{g}_y - Z_{\dot{p}} & -m\boldsymbol{g}_x - Z_{\dot{q}} & -Z_{\dot{r}} \\ -K_{\dot{u}} & -m\boldsymbol{g}_z - K_{\dot{v}} & m\boldsymbol{g}_y - K_{\dot{w}} & I_x - K_{\dot{p}} & -I_{xy} - K_{\dot{q}} & -I_{xz} - K_{\dot{r}} \\ m\boldsymbol{g}_z - M_{\dot{u}} & -M_{\dot{v}} & -m\boldsymbol{g}_x - M_{\dot{w}} & -I_{yx} - M_{\dot{p}} & I_y - M_{\dot{q}} & -I_{yz} - M_{\dot{r}} \\ -m\boldsymbol{g}_y - N_{\dot{u}} & m\boldsymbol{g}_x - N_{\dot{v}} & -N_{\dot{w}} & -I_{zx} - N_{\dot{p}} & -I_{zy} - N_{\dot{q}} & I_z - N_{\dot{r}} \end{bmatrix} \tag{56}$$

Also, the total Coriolis and centripetal matrix (39) is defined by the sum of (45) to

(53)

$$C(\boldsymbol{\nu}) = \begin{bmatrix} 0 & 0 & 0 \\ 0 & 0 & 0 \\ 0 & 0 & 0 \\ -m(\boldsymbol{g}_y q + \boldsymbol{g}_z r) & m(\boldsymbol{g}_y p + w) - Z_{\dot{w}} w & m(\boldsymbol{g}_z p - v) + Y_{\dot{v}} v \\ m(\boldsymbol{g}_x q - w) + Z_{\dot{w}} w & -m(\boldsymbol{g}_z r + \boldsymbol{g}_x p) & m(\boldsymbol{g}_z q + w) - X_{\dot{u}} u \\ m(\boldsymbol{g}_x r + v) - Y_{\dot{v}} v & m(\boldsymbol{g}_y r - u) + X_{\dot{u}} u & -m(\boldsymbol{g}_x p + \boldsymbol{g}_y q) \end{bmatrix}$$

$$\begin{bmatrix} m(\boldsymbol{g}_y q + \boldsymbol{g}_z r) & -m(\boldsymbol{g}_x q - w) - Z_{\dot{w}} w & -m(\boldsymbol{g}_x r + v) + Y_{\dot{v}} v \\ -m(\boldsymbol{g}_y p + w) + Z_{\dot{w}} w & m(\boldsymbol{g}_z r + \boldsymbol{g}_x p) & -m(\boldsymbol{g}_y r - u) - X_{\dot{u}} u \\ -m(\boldsymbol{g}_z p - v) - Y_{\dot{v}} v & -m(\boldsymbol{g}_z q + u) + X_{\dot{u}} u & m(\boldsymbol{g}_x p + \boldsymbol{g}_y q) \\ 0 & -I_{yz} q - I_{xz} p + I_z r - N_{\dot{r}} r & I_{yz} r + I_{xy} p - I_y q + M_{\dot{q}} q \\ I_{yz} q + I_{xz} p - I_z r + N_{\dot{r}} r & 0 & -I_{xz} r - I_{xy} q + I_x p - K_{\dot{p}} p \\ -I_{yz} r - I_{xy} p + I_y q - M_{\dot{q}} q & I_{xz} r + I_{xy} q - I_x p + K_{\dot{p}} p & 0 \end{bmatrix} \tag{57}$$

There are others damping effects that should be considered

$$\boldsymbol{\tau}_D = -D_S(\boldsymbol{\nu})\boldsymbol{\nu} - D_W(\boldsymbol{\nu})\boldsymbol{\nu} - D_M(\boldsymbol{\nu})\boldsymbol{\nu} \tag{58}$$

where $-D_S(\boldsymbol{\nu})\boldsymbol{\nu}$ is the skin friction, $-D_W(\boldsymbol{\nu})\boldsymbol{\nu}$ is the wave drift damping and $-D_M(\boldsymbol{\nu})\boldsymbol{\nu}$ is the damping due to vortex shedding.

Therefore, substituting Equations (50) and (58) in (49), this implies that the hydrodynamic forces and moments can be written as

$$\boldsymbol{\tau}_H = -M_A \dot{\boldsymbol{\nu}} - C_A(\boldsymbol{\nu})\boldsymbol{\nu} - D(\boldsymbol{\nu})\boldsymbol{\nu} - g(\boldsymbol{p}_o) \tag{59}$$

.

Similarly to (54) and (55), the damping effects acting in an AUV are highly nonlinear and coupled at high speed. However, assuming the vehicle has three planes of symmetry and is moving at low speed, the $D(\boldsymbol{\nu})$ matrix approximation can be defined as

$$D(\boldsymbol{\nu}) = -\begin{bmatrix} X_u & 0 & 0 & 0 & 0 & 0 \\ 0 & Y_v & 0 & 0 & 0 & 0 \\ 0 & 0 & Z_w & 0 & 0 & 0 \\ 0 & 0 & 0 & K_p & 0 & 0 \\ 0 & 0 & 0 & 0 & M_q & 0 \\ 0 & 0 & 0 & 0 & 0 & N_r \end{bmatrix} - \begin{bmatrix} X_{u|u|}|u| & 0 & 0 & 0 & 0 & 0 \\ 0 & Y_{v|v|}|v| & 0 & 0 & 0 & 0 \\ 0 & 0 & Z_{w|w|}|w| & 0 & 0 & 0 \\ 0 & 0 & 0 & K_{p|p|}|p| & 0 & 0 \\ 0 & 0 & 0 & 0 & M_{q|q|}|q| & 0 \\ 0 & 0 & 0 & 0 & 0 & N_{r|r|}|r| \end{bmatrix} \tag{60}$$

where the damping matrix is separated on linear and quadratic damping terms.

The gravitational force f_G is performed through the center of gravity $\boldsymbol{r}_G = [\boldsymbol{g}_x, \boldsymbol{g}_y, \boldsymbol{g}_z]'$ of the vehicle, while the buoyant force f_B acts through the center of buoyancy $\boldsymbol{r}_B = [\boldsymbol{b}_x, \boldsymbol{b}_y, \boldsymbol{b}_z]'$. In hydrodynamic, they are called restoring forces and play an important role to the model. By strategically projecting f_G and $\boldsymbol{r}_G$ positions, one may provide restoring moment in pitch and roll, which is useful for underactuated vehicles and safety reasons. The restoring forces are described by

$$g(\boldsymbol{p}_o) = \begin{bmatrix} (W-B)\sin\theta \\ -(W-B)\cos\theta\sin\phi \\ -(W-B)\cos\theta\cos\phi \\ \boldsymbol{g}_z W\cos\theta\sin\phi \\ \boldsymbol{g}_z W\sin\theta \\ 0 \end{bmatrix}, \tag{61}$$

where W is the weight and B the buoyancy force of the vehicle.

3.5 Dynamic Equations of LAUV

The Light Autonomous Underwater Vehicle, Figure 1, is a low-cost torpedo shaped vehicle developed for oceanographic and environmental surveys (Silva and Sousa, 2008). The dynamic model, based on (34) and (37), is given by

$$\dot{\eta}(t) = -\frac{1}{2}\epsilon(t)'\boldsymbol{\omega}(t) \tag{62a}$$

$$\dot{\epsilon}(t) = \frac{1}{2}(\eta(t)I_{3\times 3} + S(\epsilon(t)))\boldsymbol{\omega}(t) \tag{62b}$$

$$M\dot{\boldsymbol{\nu}}(t) = -C(\boldsymbol{\nu}(t))\boldsymbol{\nu}(t) - D(\boldsymbol{\nu}(t))\boldsymbol{\nu}(t) - g(\eta) + \boldsymbol{\tau}(t) \tag{62c}$$

where $M \in \mathbb{R}^{6\times 6}$, $C \in \mathbb{R}^{6\times 6}$ and $D \in \mathbb{R}^{6\times 6}$.

In contrast to Section 3.4, the studied vehicle cannot be considered symmetric on the three-planes, as a result of the torpedo shape. However, considering that the vehicle is port/starboard and top/bottom symmetric in shape and assuming the distribution of mass of a prolate ellipsoid, the inertia matrix of the LAUV will be described as

$$M = \begin{bmatrix} m - X_{\dot{u}} & 0 & 0 & 0 & m\boldsymbol{g}_z & 0 \\ 0 & m - Y_{\dot{v}} & 0 & -m\boldsymbol{g}_z & 0 & 0 \\ 0 & 0 & m - Z_{\dot{w}} & 0 & 0 & 0 \\ 0 & -m\boldsymbol{g}_z & 0 & I_x - K_{\dot{p}} & 0 & 0 \\ m\boldsymbol{g}_z & 0 & 0 & 0 & I_y - M_{\dot{q}} & 0 \\ 0 & 0 & 0 & 0 & 0 & I_z - N_{\dot{r}} \end{bmatrix}. \tag{63}$$

The Coriolis and centripetal matrix has the following expression

$$C(\boldsymbol{\nu}) = \begin{bmatrix} 0 & 0 & 0 \\ 0 & 0 & 0 \\ 0 & 0 & 0 \\ -m\boldsymbol{g}_z r & (m - Z_{\dot{w}})w & m\boldsymbol{g}_z p - (m - Y_{\dot{v}})v \\ -(m - Z_{\dot{w}})w & -m\boldsymbol{g}_z r & m\boldsymbol{g}_z q + (m - X_{\dot{u}})u \\ (m - Y_{\dot{v}})v & -(m - X_{\dot{u}})u & 0 \end{bmatrix}$$
$$\begin{bmatrix} m\boldsymbol{g}_z r & (m - Z_{\dot{w}})w & -(m - Y_{\dot{v}})v \\ -(m - Z_{\dot{w}})w & m\boldsymbol{g}_z r & (m - X_{\dot{u}})u \\ -m\boldsymbol{g}_z p + (m - Y_{\dot{v}})v & -m\boldsymbol{g}_z q - (m - X_{\dot{u}})u & 0 \\ 0 & (I_z - N_{\dot{r}})r & -(I_y - M_{\dot{q}})q \\ -(I_z - N_{\dot{r}})r & 0 & (I_x - K_{\dot{p}})p \\ (I_y - M_{\dot{q}})q & -(I_x - K_{\dot{p}})p & 0 \end{bmatrix}. \tag{64}$$

The damping matrix is given by

$$
\begin{aligned}
D(\boldsymbol{\nu}) = &-\begin{bmatrix} X_u & 0 & 0 & 0 & 0 & 0 \\ 0 & Y_v & 0 & 0 & 0 & Y_r \\ 0 & 0 & Z_w & 0 & Z_q & 0 \\ 0 & 0 & 0 & K_p & 0 & 0 \\ 0 & 0 & M_w & 0 & M_q & 0 \\ 0 & N_v & 0 & 0 & 0 & N_r \end{bmatrix} \\
&-\begin{bmatrix} X_{u|u|}|u| & 0 & 0 & 0 & 0 & 0 \\ 0 & Y_{v|v|}|v| & 0 & 0 & 0 & Y_{r|r|}|r| \\ 0 & 0 & Z_{w|w|}|w| & 0 & Z_{q|q|}|q| & 0 \\ 0 & 0 & 0 & K_{p|p|}|p| & 0 & 0 \\ 0 & 0 & M_{w|w|}|w| & 0 & M_{q|q|}|q| & 0 \\ 0 & N_{v|v|}|v| & 0 & 0 & 0 & N_{r|r|}|r| \end{bmatrix}.
\end{aligned} \tag{65}
$$

It is usual to design AUVs slightly buoyant, in order to provide easily rescue, so that the center of gravity is slightly below the center of buoyancy, providing a restoring moment in pitch and roll. Even though the original LAUV features this, we will consider them in the same position avoiding the component $g(\eta_2)$.

3.6 Actuator system mapping

The actuator system of this torpedo includes 1 propeller and 3 fins, where 1 is vertical and the other two arranged 120 degrees from each other, as shown in Figure 5. The propeller is directly responsible for the thrust force that moves the vehicle on surge, while fins are mainly responsible for leading rotational motions in yaw and pitch, as gyratory, diving and rising (Liang et al., 2013).

In this work, we will not consider the dynamics of the thruster motor and fin servos since they are typically much faster then the remaining dynamics. The relation between the command signals u_1, u_2, u_3, u_4 sent to each individual motor and the torques $\boldsymbol{\tau}(t)$ and thrust F applied to the vehicle can be mapped by means of an appropriate Jacobian matrix. The control inputs can be computed by the following equation

Figure 5: Actuators arrangement of the Light Autonomous Underwater Vehicle (LAUV)

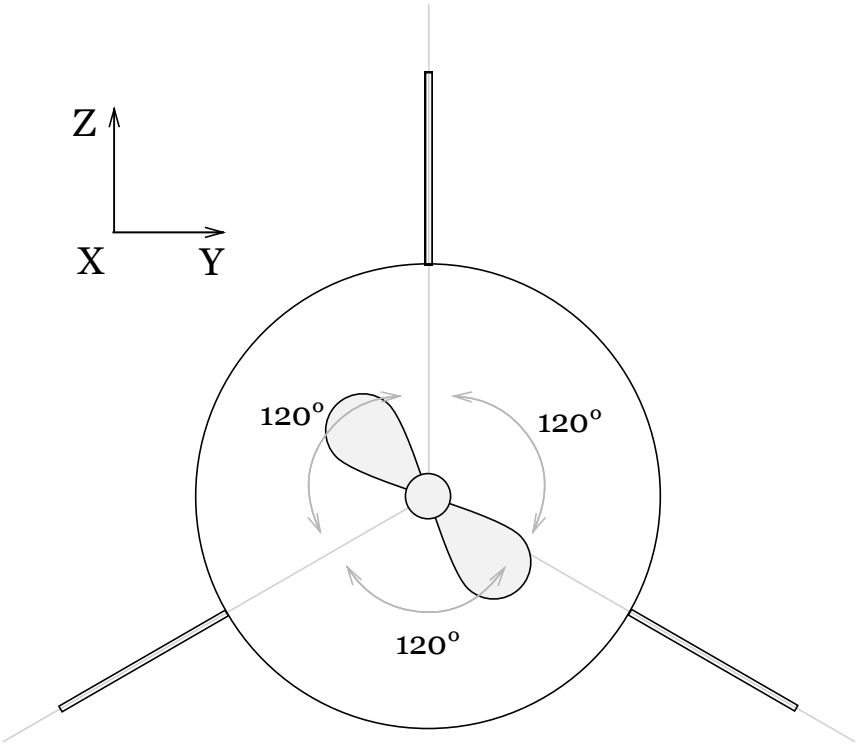

Source: the autor (2018).

$$\begin{bmatrix} u_1 \\ u_2 \\ u_3 \\ u_4 \end{bmatrix} = J^{-1} \begin{bmatrix} F \\ \boldsymbol{\tau}_1 \\ \boldsymbol{\tau}_2 \\ \boldsymbol{\tau}_3 \end{bmatrix} \tag{66}$$

where $J \in \mathbb{R}^{4\times4}$ and u_i are the control inputs.

3.7 Differential Algebraic Representation

The Differential Algebraic Representation (DAR), discussed in Section 2.5, makes use of an auxiliary vector ξ. The DAR representation is given by

$$\dot{\boldsymbol{x}} = A_1(\boldsymbol{x})\boldsymbol{x} + A_2(\boldsymbol{x})\xi(\boldsymbol{x}) + B\boldsymbol{\tau} \tag{67a}$$

$$0 = \Omega_1(\boldsymbol{x})\boldsymbol{x} + \Omega_2(\boldsymbol{x})\xi(\boldsymbol{x}) \tag{67b}$$

In order to represent system (62) in the above form, first, we make the simplifying assumption that the vehicle is at rest or at least moving at low speed and has three planes of symmetry such that M is a diagonal matrix.

From quaternion definition it follows that the equilibrium point of system (62) are

$$\boldsymbol{q}^* = \begin{bmatrix} \eta^* \\ \epsilon^* \end{bmatrix} = \begin{bmatrix} \pm 1 \\ 0 \\ 0 \\ 0 \end{bmatrix} \tag{68}$$

Furthermore, because of quaternion constraint (11), it follows that

$$\epsilon \to 0 \Longrightarrow \eta \to \pm 1 \tag{69}$$

Therefore, it suffices to ensure the convergence of ϵ to the origin in order to reach the equilibrium point $\boldsymbol{q}^*$. As a consequence, the dynamics of $\dot{\eta}$ shall be dropped from the DAR.

Also, the following change of coordinates will be performed

$$\varepsilon = \text{sign}(\eta)\epsilon \tag{70}$$

whose time derivative is given by

$$\dot{\varepsilon} = \text{sign}(\eta)\dot{\epsilon} + \delta_D(\eta)\dot{\eta}\epsilon \tag{71}$$

In order to avoid the discontinuity of the Dirac delta $\delta_D(\eta)$, this work will limit its analysis to the domain given by

$$\eta \in [-1, 1] - \{0\}. \tag{72}$$

In this domain, the system may be describe as

$$\begin{aligned}\dot{\varepsilon} &= \frac{1}{2}(|\eta|\, I_{3\times 3} + S(\varepsilon))\boldsymbol{\omega} \\ \dot{\boldsymbol{\omega}} &= -M^{-1}(C(\boldsymbol{\omega}) + D(\boldsymbol{\omega}))\boldsymbol{\omega} + M^{-1}\boldsymbol{\tau}\end{aligned} \tag{73}$$

where

$$M = \begin{bmatrix} I_x - K_{\dot{p}} & 0 & 0 \\ 0 & I_y - M_{\dot{q}} & 0 \\ 0 & 0 & I_z - N_{\dot{r}} \end{bmatrix} = \begin{bmatrix} M_1 & 0 & 0 \\ 0 & M_2 & 0 \\ 0 & 0 & M_3 \end{bmatrix}, \tag{74}$$

$$C(\boldsymbol{\omega}) = \begin{bmatrix} 0 & (I_z - N_{\dot{r}})\boldsymbol{\omega}_3 & -(I_y - M_{\dot{q}})\boldsymbol{\omega}_2 \\ -(I_z - N_{\dot{r}})\boldsymbol{\omega}_3 & 0 & (I_x - K_{\dot{p}})\boldsymbol{\omega}_1 \\ (I_y - M_{\dot{q}})\boldsymbol{\omega}_2 & -(I_x - K_{\dot{p}})\boldsymbol{\omega}_1 & 0 \end{bmatrix}, \tag{75}$$

$$D(\boldsymbol{\omega}) = D_l + D_q\boldsymbol{\omega} = -\begin{bmatrix} K_p & 0 & 0 \\ 0 & M_q & 0 \\ 0 & 0 & N_r \end{bmatrix} - \begin{bmatrix} K_{p|p|}|\boldsymbol{\omega}_1| & 0 & 0 \\ 0 & M_{q|q|}|\boldsymbol{\omega}_2| & 0 \\ 0 & 0 & N_{r|r|}|\boldsymbol{\omega}_3| \end{bmatrix} \tag{76}$$

Note that the change of coordinates in (70) replaced $\eta(t)$ in the second equation of (62), by $\left|\eta(t)\right|$ in (73). Also, in order to organize the notation, when we describe the system in DAR we will use $\omega = [p, q, r] \rightarrow \boldsymbol{\omega} = [\boldsymbol{\omega}_1, \boldsymbol{\omega}_2, \boldsymbol{\omega}_3]$ and $\varepsilon = [\varepsilon_1, \varepsilon_2, \varepsilon_3]$.

Thus, the natural choice of state variables given by

$$\boldsymbol{x} = \begin{bmatrix} \varepsilon_1 & \varepsilon_2 & \varepsilon_3 & \boldsymbol{\omega}_1 & \boldsymbol{\omega}_2 & \boldsymbol{\omega}_3 \end{bmatrix}' \tag{77}$$

allow us to represent $|\eta|$ as a function of $\boldsymbol{x}$,

$$\left|\eta(t)\right| = +\sqrt{1 - \epsilon'\epsilon} = +\sqrt{1 - \varepsilon'\varepsilon} = \delta(\boldsymbol{x}) \in (0, 1], \tag{78}$$

and also leads to choose the following as the vector of grouped nonlinear terms to be used in (67)

$$\begin{aligned}\xi(\boldsymbol{x}) = \Big[&\boldsymbol{\omega}_1\varepsilon_2 \quad \boldsymbol{\omega}_1\varepsilon_3 \quad \boldsymbol{\omega}_2\varepsilon_1 \quad \boldsymbol{\omega}_2\varepsilon_3 \quad \boldsymbol{\omega}_3\varepsilon_1 \quad \boldsymbol{\omega}_3\varepsilon_2 \\ &\boldsymbol{\omega}_1^2 \quad \boldsymbol{\omega}_2^2 \quad \boldsymbol{\omega}_3^2 \quad \boldsymbol{\omega}_1\boldsymbol{\omega}_2 \quad \boldsymbol{\omega}_1\boldsymbol{\omega}_3 \quad \boldsymbol{\omega}_2\boldsymbol{\omega}_3\Big]'.\end{aligned} \tag{79}$$

Expressing the system (73) in the DAR form (67)

$$\dot{\boldsymbol{x}} = \begin{bmatrix} 0 & 0 & 0 & \delta(\boldsymbol{x})/2 & 0 & 0 \\ 0 & 0 & 0 & 0 & \delta(\boldsymbol{x})/2 & 0 \\ 0 & 0 & 0 & 0 & 0 & \delta(\boldsymbol{x})/2 \\ 0 & 0 & 0 & \frac{-K_p}{I_x - K_{\dot{p}}} & 0 & 0 \\ 0 & 0 & 0 & 0 & \frac{-M_q}{I_y - M_{\dot{q}}} & 0 \\ 0 & 0 & 0 & 0 & 0 & \frac{-N_r}{I_z - N_{\dot{r}}} \end{bmatrix} \begin{bmatrix} \varepsilon_1 \\ \varepsilon_2 \\ \varepsilon_3 \\ \boldsymbol{\omega}_1 \\ \boldsymbol{\omega}_2 \\ \boldsymbol{\omega}_3 \end{bmatrix} + \begin{bmatrix} 0 & 0 & 0 & -\frac{1}{2} & 0 & \frac{1}{2} \\ 0 & \frac{1}{2} & 0 & 0 & -\frac{1}{2} & 0 \\ -\frac{1}{2} & 0 & \frac{1}{2} & 0 & 0 & 0 \\ 0 & 0 & 0 & 0 & 0 & 0 \\ 0 & 0 & 0 & 0 & 0 & 0 \\ 0 & 0 & 0 & 0 & 0 & 0 \end{bmatrix}$$

$$\begin{bmatrix} 0 & 0 & 0 & 0 & 0 & 0 \\ 0 & 0 & 0 & 0 & 0 & 0 \\ 0 & 0 & 0 & 0 & 0 & 0 \\ \frac{-K_{\dot{p}|p|}}{M_1} & 0 & 0 & 0 & 0 & \frac{M_3 - M_2}{M_1} \\ 0 & \frac{-M_{\dot{q}|q|}}{M_2} & 0 & 0 & \frac{M_1 - M_3}{M_2} & 0 \\ 0 & 0 & \frac{-N_{\dot{r}|r|}}{M_3} & \frac{M_2 - M_1}{M_3} & 0 & 0 \end{bmatrix} \begin{bmatrix} \boldsymbol{\omega}_1\varepsilon_2 \\ \boldsymbol{\omega}_1\varepsilon_3 \\ \boldsymbol{\omega}_2\varepsilon_1 \\ \boldsymbol{\omega}_2\varepsilon_3 \\ \boldsymbol{\omega}_3\varepsilon_1 \\ \boldsymbol{\omega}_3\varepsilon_2 \\ \boldsymbol{\omega}_1^2 \\ \boldsymbol{\omega}_2^2 \\ \boldsymbol{\omega}_3^2 \\ \boldsymbol{\omega}_1\boldsymbol{\omega}_2 \\ \boldsymbol{\omega}_1\boldsymbol{\omega}_3 \\ \boldsymbol{\omega}_2\boldsymbol{\omega}_3 \end{bmatrix} + \begin{bmatrix} 0_{3\times 3} \\ M^{-1} \end{bmatrix} \boldsymbol{\tau}, \tag{80}$$

$$0 = - \begin{bmatrix} 0 & 0 & 0 & \varepsilon_2 & 0 & 0 \\ 0 & 0 & 0 & \varepsilon_3 & 0 & 0 \\ 0 & 0 & 0 & 0 & \varepsilon_1 & 0 \\ 0 & 0 & 0 & 0 & \varepsilon_3 & 0 \\ 0 & 0 & 0 & 0 & 0 & \varepsilon_1 \\ 0 & 0 & 0 & 0 & 0 & \varepsilon_2 \\ 0 & 0 & 0 & \boldsymbol{\omega}_1 & 0 & 0 \\ 0 & 0 & 0 & 0 & \boldsymbol{\omega}_2 & 0 \\ 0 & 0 & 0 & 0 & 0 & \boldsymbol{\omega}_3 \\ 0 & 0 & 0 & 0 & \boldsymbol{\omega}_1 & 0 \\ 0 & 0 & 0 & \boldsymbol{\omega}_3 & 0 & 0 \\ 0 & 0 & 0 & 0 & 0 & \boldsymbol{\omega}_2 \end{bmatrix} \begin{bmatrix} \varepsilon_1 \\ \varepsilon_2 \\ \varepsilon_3 \\ \boldsymbol{\omega}_1 \\ \boldsymbol{\omega}_2 \\ \boldsymbol{\omega}_3 \end{bmatrix} + I_{12\times 12} \begin{bmatrix} \boldsymbol{\omega}_1\varepsilon_2 \\ \boldsymbol{\omega}_1\varepsilon_3 \\ \boldsymbol{\omega}_2\varepsilon_1 \\ \boldsymbol{\omega}_2\varepsilon_3 \\ \boldsymbol{\omega}_3\varepsilon_1 \\ \boldsymbol{\omega}_3\varepsilon_2 \\ \boldsymbol{\omega}_1^2 \\ \boldsymbol{\omega}_2^2 \\ \boldsymbol{\omega}_3^2 \\ \boldsymbol{\omega}_1\boldsymbol{\omega}_2 \\ \boldsymbol{\omega}_1\boldsymbol{\omega}_3 \\ \boldsymbol{\omega}_2\boldsymbol{\omega}_3 \end{bmatrix}. \tag{81}$$

Given the above, the system can be described by the following matrices

$$\dot{\boldsymbol{x}} = A_1(\boldsymbol{x})\boldsymbol{x} + A_2(\boldsymbol{x})\xi(\boldsymbol{x}) + B\boldsymbol{\tau}$$

$$0 = \Omega_1(\boldsymbol{x})\boldsymbol{x} + \Omega_2(\boldsymbol{x})\xi(\boldsymbol{x})$$

where

$$A_1(\boldsymbol{x}) = \begin{bmatrix} 0 & 0 & 0 & \delta(\boldsymbol{x})/2 & 0 & 0 \\ 0 & 0 & 0 & 0 & \delta(\boldsymbol{x})/2 & 0 \\ 0 & 0 & 0 & 0 & 0 & \delta(\boldsymbol{x})/2 \\ 0 & 0 & 0 & \frac{-K_p}{I_x - K_{\dot{p}}} & 0 & 0 \\ 0 & 0 & 0 & 0 & \frac{-M_q}{I_y - M_{\dot{q}}} & 0 \\ 0 & 0 & 0 & 0 & 0 & \frac{-N_r}{I_z - N_{\dot{r}}} \end{bmatrix} \tag{82}$$

$$A_2 = \begin{bmatrix} 0 & 0 & 0 & -\frac{1}{2} & 0 & \frac{1}{2} & 0 & 0 & 0 & 0 & 0 & 0 \\ 0 & \frac{1}{2} & 0 & 0 & -\frac{1}{2} & 0 & 0 & 0 & 0 & 0 & 0 & 0 \\ -\frac{1}{2} & 0 & \frac{1}{2} & 0 & 0 & 0 & 0 & 0 & 0 & 0 & 0 & 0 \\ 0 & 0 & 0 & 0 & 0 & 0 & \frac{-K_{p|p|}}{M_1} & 0 & 0 & 0 & 0 & \frac{M_3 - M_2}{M_1} \\ 0 & 0 & 0 & 0 & 0 & 0 & 0 & \frac{-M_{q|q|}}{M_2} & 0 & 0 & \frac{M_1 - M_3}{M_2} & 0 \\ 0 & 0 & 0 & 0 & 0 & 0 & 0 & 0 & \frac{-N_{r|r|}}{M_3} & \frac{M_2 - M_1}{M_3} & 0 & 0 \end{bmatrix} \tag{83}$$

$$B = \begin{bmatrix} 0_{3\times 3} \\ M^{-1} \end{bmatrix} \tag{84}$$

$$\Omega_1(\boldsymbol{x}) = -\begin{bmatrix} 0 & 0 & 0 & \varepsilon_2 & 0 & 0 \\ 0 & 0 & 0 & \varepsilon_3 & 0 & 0 \\ 0 & 0 & 0 & 0 & \varepsilon_1 & 0 \\ 0 & 0 & 0 & 0 & \varepsilon_3 & 0 \\ 0 & 0 & 0 & 0 & 0 & \varepsilon_1 \\ 0 & 0 & 0 & 0 & 0 & \varepsilon_2 \\ 0 & 0 & 0 & \boldsymbol{\omega}_1 & 0 & 0 \\ 0 & 0 & 0 & 0 & \boldsymbol{\omega}_2 & 0 \\ 0 & 0 & 0 & 0 & 0 & \boldsymbol{\omega}_3 \\ 0 & 0 & 0 & 0 & \boldsymbol{\omega}_1 & 0 \\ 0 & 0 & 0 & \boldsymbol{\omega}_3 & 0 & 0 \\ 0 & 0 & 0 & 0 & 0 & \boldsymbol{\omega}_2 \end{bmatrix} \tag{85}$$

$$\Omega_2 = I_{12\times 12} \tag{86}$$

The dynamics of system (73) can be readily recovered by

$$\dot{x} = (A_1(\boldsymbol{x}) - A_2\Omega_2^{-1}\Omega_1(\boldsymbol{x}))\boldsymbol{x} + B\boldsymbol{\tau} \tag{87}$$

Since $A_1(\boldsymbol{x})$ and $\Omega_1(\boldsymbol{x})$ depend on $\boldsymbol{x}$, these variables will be treated as time varying parameters in theirs respective matrices.

3.8 Domain of Interest

We know from (72) that this description is only valid for $\eta \neq 0$, in order to avoid the discontinuity. Therefore, the domain of interest that will be analysed in this work is given by

$$\mathcal{X} = \{\boldsymbol{x} \in \mathbb{R}^6 : \ |\boldsymbol{x}_i| \leq \sin\frac{\overline{\psi}}{2}, \ \ 0 \leq \overline{\psi} < \pi, \ \left|\boldsymbol{x}_j\right| \leq \overline{\boldsymbol{\omega}}\}, \tag{88}$$

for $i = 1, 2, 3$ and $j = 4, 5, 6$. The value of $\overline{\boldsymbol{\omega}}$ that bounds the angular velocities will be defined later.

4 Analysis and Control Design

The main problem addressed in this work is that of providing linear tools for the analysis and control design of the orientation of an Autonomous Underwater Vehicle described by equations (62). This Chapter aims to achieve the stability of the origin of the system in the form (67) described in the previous chapter. First, we will assess mathematically the stability of the system proving a theorem that satisfies all LMIs from Lemma 2.1. Then, a control design strategy will be provided in order to compute gain K such that the closed loop system is locally exponentially stable.

4.1 Analysis

In order to achieve the Lyapunov stability of the Autonomous Underwater Vehicle's origin, consider the following control law

$$\boldsymbol{\tau} = K\boldsymbol{x} \tag{89}$$

where $K = [K_1, K_2] \in \mathbb{R}^{3\times 6}$ and $\boldsymbol{x} = [\epsilon'\boldsymbol{\omega}'] \in \mathbb{R}^6$.

Therefore, the vehicle torques are governed by

$$\boldsymbol{\tau} = K_1 \operatorname{sign}(\eta)\epsilon + K_2\boldsymbol{\omega} \tag{90}$$

control law.

The following theorem adapted from the work by (Coutinho et al., 2004), provides sufficient conditions for the local exponential stability of the closed loop system. Due to the DAR of the system, these conditions are given by constraints in the form of Linear Matrix Inequalities.

The solution to this problem is presented in theorem

Theorem 4.1. *Consider system (62) and its DAR representation (67) subject to control law (89) for a given $K \in \mathbb{R}^{3\times 6}$. Suppose there is a positive definite matrix $P = P' \in \mathbb{R}^{6\times 6}$ and a matrix $L \in \mathbb{R}^{12\times 6}$ that satisfy the following inequatilies for all $\boldsymbol{x}$ evaluated at vertices $\mathcal{V}(\mathcal{X})$*

$$P > 0 \tag{91}$$

$$\begin{bmatrix} He\{P(A_1(\boldsymbol{x}) + BK)\} & PA_2 \\ \star & 0 \end{bmatrix} + \Omega(\boldsymbol{x})'L' + L\Omega(x) < 0 \tag{92}$$

$$\begin{bmatrix} 1 & \alpha_i^{-1}\mathbf{i}_i \\ \alpha_i^{-1}\mathbf{i}_i' & P \end{bmatrix} \geq 0, \quad i = 1, 2, 3 \tag{93}$$

where $\Omega = [\Omega_1, \Omega_2]$ *and* $\alpha = \sin(\overline{\psi}/2)$. *Then,* $\boldsymbol{x} = 0$ *is an exponentially stable point of the closed loop system and an estimate of its region of attraction is given by*

$$\mathcal{R}_a = \{\boldsymbol{x} \in \mathbb{R}^6 : \boldsymbol{x}'P\boldsymbol{x} \leq 1\}. \tag{94}$$

■

Proof. All conditions of Lemma 2.1 are proved below:

Constraint (28): Select the following Lyapunov candidate function

$$V(\boldsymbol{x}) = \boldsymbol{x}'P\boldsymbol{x}. \tag{95}$$

Then, from the assumption (91) and Definition 2.2 we conclude that

$$V(\boldsymbol{x}) > 0 \tag{96}$$

is positive definite. Therefore, picking the smallest and largest eigenvalues of P for k_1, k_2, respectively, we have that the first matrix inequality of Lemma 2.1 is satisfied.

Constraint (29): Since the required condition is a non strict inequality, we will add a small positive scalar to (92) as following

$$\begin{bmatrix} \mathrm{He}\{P(A_1(\boldsymbol{x}) + BK)\} & PA_2 \\ \star & 0 \end{bmatrix} + \Omega(\boldsymbol{x})'L' + L\Omega(x) + k_3 \begin{bmatrix} I_{6\times 6} \\ 0_{12\times 6} \end{bmatrix} \begin{bmatrix} I_{6\times 6} & 0_{6\times 12} \end{bmatrix} \leq 0. \tag{97}$$

.

Taking the following auxiliary vector

$$\zeta_1 = \begin{bmatrix} \boldsymbol{x} \\ \xi \end{bmatrix} \tag{98}$$

then, it follows that $\Omega(\boldsymbol{x})\zeta_1 = 0$. By pre- and post-multiplying (97) by (98) we find that

$$\zeta_1' \begin{bmatrix} \mathrm{He}\{P(A_1(\boldsymbol{x}) + BK)\} & PA_2 \\ \star & 0 \end{bmatrix} \zeta_1 \leq -k_3 \boldsymbol{x}'\boldsymbol{x}. \tag{99}$$

Given the closed loop system (16) subject to the control law (89), we have that inequality (99) becomes

$$\dot{\boldsymbol{x}}' P \boldsymbol{x} + \boldsymbol{x}' P \dot{\boldsymbol{x}} \leq -k_3 \boldsymbol{x}'\boldsymbol{x} \tag{100}$$

which satisfies (29).

Constraint (30): If we pre- and post-multiplying (93) by

$$\zeta_2 = \begin{bmatrix} 1 \\ \boldsymbol{x} \end{bmatrix} \tag{101}$$

and its transpose, it follows that

$$\zeta_2' \begin{bmatrix} 1 & \alpha_i^{-1}\mathbf{i}_i \\ \alpha_i^{-1}\mathbf{i}_i' & P \end{bmatrix} \zeta_2 \geq 0, \quad i = 1, 2, 3. \tag{102}$$

Considering that $\boldsymbol{x}_i = \mathbf{i}_i \boldsymbol{x}$, the equation above is equivalent to

$$2 - 2\alpha^{-1}\boldsymbol{x}_i + (\boldsymbol{x}' P \boldsymbol{x} - 1) \geq 0, \quad i = 1, 2, 3. \tag{103}$$

Accordingly to S-Procedure, presented in Section 2.6.2, if we can describe equation (103) in form (26) with a nonnegative λ

$$1 - \alpha^{-1}\boldsymbol{x}_i > \lambda(1 - \boldsymbol{x}' P \boldsymbol{x}), \quad \lambda = 2, \tag{104}$$

we can assume that

$$\alpha^{-1}|\boldsymbol{x}_i| \leq 1, \quad \forall \boldsymbol{x} : \boldsymbol{x}' P \boldsymbol{x} \leq 1, \quad i = 1, 2, 3 \tag{105}$$

what satisfies conditions (30) and (88) by defining that $\alpha = \sin(\frac{\bar{\psi}}{2})$. In other words, it means that the estimate domain of attraction of the origin $\mathcal{R} \subset \mathcal{X}$.

This theorem gives a estimate of region of attraction since the linear matrix inequalities (92) and (93) are verified in a finite set of points represented by the vertices $\mathcal{V}(\mathcal{X})$, then, by convexity, Section 2.3, they are also satisfied for all $\boldsymbol{x} \in \mathcal{X}$. Also, if LMI (93) guarantees $\mathcal{R}_a \subset \mathcal{X}$, it follows that (91), (92), (93), (94) imply the conditions of Lemma 2.1, which

completes the proof. □

In order to maximize the estimate of region of attraction $\mathcal{R}_a$, we may minimize the trace of the Lyapunov matrix P (Boyd et al., 1994). Then, the task of maximization may be defined by the following semidefinite optimization problem

$$\begin{aligned} &\underset{P,L}{\text{minimize}} && \text{trace}(P) \\ &\text{subject to} && (91), (92) \text{ and } (93) \end{aligned} \tag{106}$$

where P and L are the decision variables.

In the next section, we will evaluate the gain K that stabilizes the system.

4.2 Control Design (Semidefinite Optimization Problem)

This section will provide a design strategy for the closed loop system in order to compute gain K such that it is locally exponentially stable. The following theorem, adapted from the work by (Oliveira et al., 2012), provides sufficient conditions for that through constraints in the form of linear matrix inequalities.

Theorem 4.2. *Consider system (62) and its DAR representation (67) subject to control law (89) for a given $K \in \mathbb{R}^{3\times 6}$. Suppose there is a positive definite constant matrix $Q_2 = Q_2' \in \mathbb{R}^{6\times 6}$, nonsingular matrices $Q_1 \in \mathbb{R}^{6\times 6}$ and $Q_3 \in \mathbb{R}^{9\times 9}$, and a matrix $Y \in \mathbb{R}^{3\times 6}$ that satisfy the following inequalities for all $\boldsymbol{x}$ evaluated at $\mathcal{X}$*

$$Q_2 > 0 \tag{107a}$$

$$\begin{bmatrix} -Q_1' - Q_1 & A_1(x)Q_2' + BY & A_2Q_3' \\ \star & He\{A_1(x)Q_2' + BY\} & A_2Q_3' + Q_2\Omega_1' \\ \star & \star & He\{\Omega_2 Q_3'\} \end{bmatrix} < 0 \tag{107b}$$

$$\begin{bmatrix} 1 & \alpha_i^{-1}\boldsymbol{i}_i Q_2 \\ \alpha_i^{-1} Q_2 \boldsymbol{i}_i & P \end{bmatrix} \geq 0, i = 1, 2, 3 \tag{107c}$$

Then, $\boldsymbol{x} = 0$ is an exponentially stable equilibrium point of the closed loop system (62) subject to (89) with $K = YQ^{-1}$. Furthermore, the trajectory $x(t)$ belongs to $\mathcal{R}_d$, approaches the origin when $t \to \infty$, and an estimate of its region of attraction is given by

$$\mathcal{R}_d = \{\boldsymbol{x} \in \mathbb{R}^6 : \boldsymbol{x}' Q_2^{-1} \boldsymbol{x} \leq 1\}. \tag{108}$$

□

Proof. All conditions of Lemma 2.1 are achieved by the following constraints:

Constraint (28): Take the same Lyapunov candidate function as before

$$V(\boldsymbol{x}) = \boldsymbol{x}' P \boldsymbol{x}. \tag{109}$$

Defining that

$$P = Q_2^{-1} \tag{110}$$

from the assumption (107a) and Definition 2.2 we conclude that Q_2 is positive definite, consequently nonsingular and inversible, what holds condition (28).

Constraint (29): if we express constraint (107b) in terms of an auxiliary matrix

$$\zeta_3 = \begin{bmatrix} Q_1 & 0 & 0 \\ 0 & Q_2 & 0 \\ 0 & 0 & Q_3 \end{bmatrix} \tag{111}$$

it follows that the linear matrix inequality (107b) is equivalent to

$$\zeta_3' \Lambda_2 \zeta_3 = \begin{bmatrix} Q_1' \Lambda_{2_{11}} Q_1 & Q_1' \Lambda_{2_{12}} Q_2 & Q_1' \Lambda_{2_{13}} Q_3 \\ Q_2' \Lambda_{2_{21}} Q_1 & Q_2' \Lambda_{2_{22}} Q_2 & Q_2' \Lambda_{2_{23}} Q_3 \\ Q_3' \Lambda_{2_{31}} Q_1 & Q_3' \Lambda_{2_{32}} Q_2 & Q_3' \Lambda_{2_{33}} Q_3 \end{bmatrix} < 0 \tag{112}$$

where $\Lambda_{2_{ij}}$ for $i, j = 1, 2, 3$ are components of Λ_2.

Next, defining that $M_i \in \mathbb{R}^{6\times 6}$ for $i = 1, 2, 3$, $P = M_2$, $Q_i = M_i^{-1}$, $A_{1cl} = A_1 + BK$, and simplifying the notation by writing A_1 instead of $A_1(\boldsymbol{x})$, we find that the components of Λ_2 are

$$\Lambda_{2_{11}} = \frac{-Q_1' - Q_1}{Q_1 Q_1'} = -M_1 - M_1', \tag{113}$$

$$\Lambda_{2_{12}} = \frac{A_1 Q_2' + BKQ_2}{Q_1 Q_2'} = M_1 A_{1cl}(\boldsymbol{x}) = P - P + M_1 A_{1cl}(\boldsymbol{x}) = P - M_2' + M_1 A_{1cl}(\boldsymbol{x}), \tag{114}$$

$$\Lambda_{2_{13}} = \frac{A_2 Q_3'}{Q_1 Q_3'} = M_1 A_2, \tag{115}$$

$$\Lambda_{2_{21}} = \frac{Q_2 A_1' + Y'B'}{Q_2 Q_1'} = A_{1cl}'(\boldsymbol{x}) M_1' = P - P + A_{1cl}'(\boldsymbol{x}) M_1' = P - M_2 + A_{1cl}'(\boldsymbol{x}) M_1', \tag{116}$$

$$\Lambda_{2_{22}} = \frac{(A_1 + BK)Q_2' + Q_2(A_1' + K'B')}{Q_2 Q_2'} = He\{M_2 A_{1cl}(\boldsymbol{x})\}, \tag{117}$$

$$\Lambda_{2_{23}} = \frac{A_2 Q_3' + Q_2 \Omega_1'}{Q_2 Q_3'} = M_2 A_2 + \Omega_1' M_3', \tag{118}$$

$$\Lambda_{2_{31}} = \frac{Q_3 A_2'}{Q_3 Q_1'} = A_2' M_1', \tag{119}$$

$$\Lambda_{2_{32}} = \frac{Q_3 A_2' + \Omega_1 Q_2'}{Q_3 Q_2'} = A_2' M_2' + M_3 \Omega_1, \tag{120}$$

$$\Lambda_{2_{33}} = \frac{\Omega_2 Q_3' + \Omega_2' Q_3}{Q_3 Q_3'} = He\{M_3 \Omega_2\}. \tag{121}$$

Substituting (113)-(121) into (112) we have that

$$\Lambda_2 = \begin{bmatrix} -M_1 - M_1' & P - M_2' + M_1 A_{1cl}(\boldsymbol{x}) & M_1 A_2 \\ \star & He\{M_2 A_{1cl}(\boldsymbol{x})\} & M_2 A_2 + \Omega_1' M_3' \\ \star & \star & He\{M_3 \Omega_2\} \end{bmatrix} < 0. \tag{122}$$

Since the required condition is a non strict inequality, we will add a small positive scalar to the above as we have done before, in Section 4.1.

Moreover, let us define an auxiliary vector

$$\zeta_4 = \begin{bmatrix} \dot{\boldsymbol{x}}(t) \\ \boldsymbol{x}(t) \\ \xi(t) \end{bmatrix}. \tag{123}$$

If we pre- and post-multiply Λ_2 by it, we will have that

$$\zeta_4' \Lambda_2 \zeta_4 \leq -k_3 \boldsymbol{x}' \boldsymbol{x}. \tag{124}$$

We can rewrite the above as follows

$$
\begin{aligned}
&\boldsymbol{x}'P\dot{\boldsymbol{x}} + \dot{\boldsymbol{x}}'P\boldsymbol{x} \\
&+ \dot{\boldsymbol{x}}'M_1(-\dot{\boldsymbol{x}} + A_{1cl}(\boldsymbol{x})\boldsymbol{x} + A_2\xi) \\
&+ M_1'\dot{\boldsymbol{x}}(-\dot{\boldsymbol{x}}' + A_{1cl}'(\boldsymbol{x})\boldsymbol{x} + \xi' A_2') \\
&+ \boldsymbol{x}'M_2(-\dot{\boldsymbol{x}} + A_{1cl}(\boldsymbol{x})\boldsymbol{x} + A_2\xi) \\
&+ M_2'\boldsymbol{x}(-\dot{\boldsymbol{x}}' + A_{1cl}'(\boldsymbol{x})\boldsymbol{x} + \xi' A_2') \\
&+ \xi' M_3(\Omega_1\boldsymbol{x} + \Omega_2\xi) \\
&+ M_3'\xi(\boldsymbol{x}'\Omega_1' + \xi'\Omega_2') \leq -k_3\boldsymbol{x}'\boldsymbol{x},
\end{aligned} \tag{125}
$$

and it may be expressed as

$$
\boldsymbol{x}'P\dot{\boldsymbol{x}} + \dot{\boldsymbol{x}}'P\boldsymbol{x} + \beta_1 + \beta_1' + \beta_2 + \beta_2' + \beta_3 + \beta_3' \leq -k_3\boldsymbol{x}'\boldsymbol{x}. \tag{126}
$$

Finally, defining the following scalar functions

$$
\beta_1 = \dot{\boldsymbol{x}}'M_1[-\dot{\boldsymbol{x}}(t) + A_{1cl}(\boldsymbol{x})\boldsymbol{x} + A_2\xi] = 0, \tag{127a}
$$

$$
\beta_2 = \boldsymbol{x}'M_2[-\dot{\boldsymbol{x}}(t) + A_{1cl}(\boldsymbol{x})\boldsymbol{x} + A_2\xi] = 0, \tag{127b}
$$

$$
\beta_3 = \xi' M_3[\Omega_1(\boldsymbol{x})\boldsymbol{x} + \Omega_2\xi] = 0, \tag{127c}
$$

it follows that

$$
\boldsymbol{x}'P\dot{\boldsymbol{x}} + \dot{\boldsymbol{x}}'P\boldsymbol{x} \leq -k_3\boldsymbol{x}'\boldsymbol{x}. \tag{128}
$$

Therefore, considering the quadratic Lyapunov function defined in (109), we have that

$$
\dot{V}(\boldsymbol{x}) = \dot{\boldsymbol{x}}'P\boldsymbol{x} + \boldsymbol{x}'P\dot{\boldsymbol{x}} \leq -k_3\boldsymbol{x}'\boldsymbol{x}. \tag{129}
$$

Hence, (107b) implies (126) which, in turn, satisfies (29).

Constraint (30): If we pre- and post-multiply (107c) by

$$
\begin{bmatrix} 1 & 0 \\ 0 & P \end{bmatrix} \tag{130}
$$

it will leads to the linear matrix inequality (93),

$$\begin{bmatrix} 1 & 0 \\ 0 & P \end{bmatrix}' \begin{bmatrix} 1 & \alpha_i^{-1}\mathbf{i}_i Q_2 \\ \alpha_i^{-1} Q_2 \mathbf{i}_i & P \end{bmatrix} \begin{bmatrix} 1 & 0 \\ 0 & P \end{bmatrix} = \begin{bmatrix} 1 & \alpha_i^{-1}\mathbf{i}_i \\ \alpha_i^{-1}\mathbf{i}_i' & P \end{bmatrix} \geq 0, \quad i = 1, 2, 3$$

which is already proven in the last section in Theorem 4.1. Thus, all required conditions of Lemma 2.1 are satisfied at vertices $\mathcal{V}(\mathcal{X})$ and guarantee $\mathcal{R}_d \subset \mathcal{X}$, which concludes the proof.

□

From the definition of the domain of attraction (108), it is clear that minimizing $Q_2^{-1} = P$, it implies in the maximization of $\mathcal{R}_d$. Regarding to the Schur complement, detailed in Section 2.6.1, if we chose $Q = Q_2$, $S = I_n$ and $R = N$, and apply that to (23) we have that

$$N > Q_2^{-1} = P, \tag{131}$$

therefore, minimizing the trace of N implies in the minimization of P which, in turn, implies in the maximization the region of attraction $\mathcal{R}_a$.

In order to evaluate the feedback gain K that maximizes the region of attraction $\mathcal{R}_a$, since the following optimization problem can be considered subjected to constraints in the form of linear matrix inequalities

$$\begin{aligned} &\text{minimize} && \text{trace}(N) \\ &\text{subject to} && (91), (92), (93) \quad \forall \boldsymbol{x} \in \mathcal{V}(\mathcal{X}) \text{ and } \begin{bmatrix} Q_2 & I_n \\ I_n & N \end{bmatrix} > 0. \end{aligned} \tag{132}$$

5 Results

In this chapter, it will be presented the numerical results obtained throughout the progress of this work along to the relevant information necessary for reproducing this results. First, the main simulation procedures will be described followed by the simulation and constructive parameters. Next, we will present three simulation scenarios, which this method were applied. Finally, we will discuss the obtained results.

5.1 Simulation Procedure

The numerical results were obtained from the software Matlab R2013b with the free packages: toolbox Yalmip (Lofberg, 2004) and SDPT3 solver (Toh et al., 1999). The feasibility of convex optimization problems is strongly related to the size of the region $\mathcal{X}$, thus the followed procedures leads one to investigate larger regions of attraction.

- **Step 1:** Select the intended scenario for simulation.
- **Step 2:** Increase gradually the $\overline{\psi}$ in the domain of interest (88).
- **Step 3:** Compute the gain K that maximizes the region of attraction $\mathcal{R}_d$ applying Theorem 4.2.
- **Step 4:** Apply the gain K to Theorem 4.1.
- **Step 5:** Increase the $\overline{\psi}$ again in the domain of interest (88) to investigate a larger region of attraction $\mathcal{R}_a$.

Given that, the simulation must be configured with simulation and constructive parameters in order to reproduce the intended scenarios. The following section presents all the required configurations.

5.2 Simulation Parameters

Now that the simulation method is structured and declared step by step, several fundamental constants are necessary to be defined. The Light Autonomous Underwater Vehicle used in this study, depicted side by side with the ISURUS in Figure 6, is a torpedo shaped vehicle with a length (l) of 108cm, diameter (d) of 15cm and mass (m)

of approximately 18kg. The actuator system is composed by one propeller and three fins, where one is vertical and the other two arranged ±120 degrees from each other, as shown in Figure 5. The propeller is positioned at the aft end of the AUV, while the fins are placed $x_{fin} = -40cm$ from the center of buoyancy.

Figure 6: ISURUS (top) and LAUV (bottom) side by site, at USTL

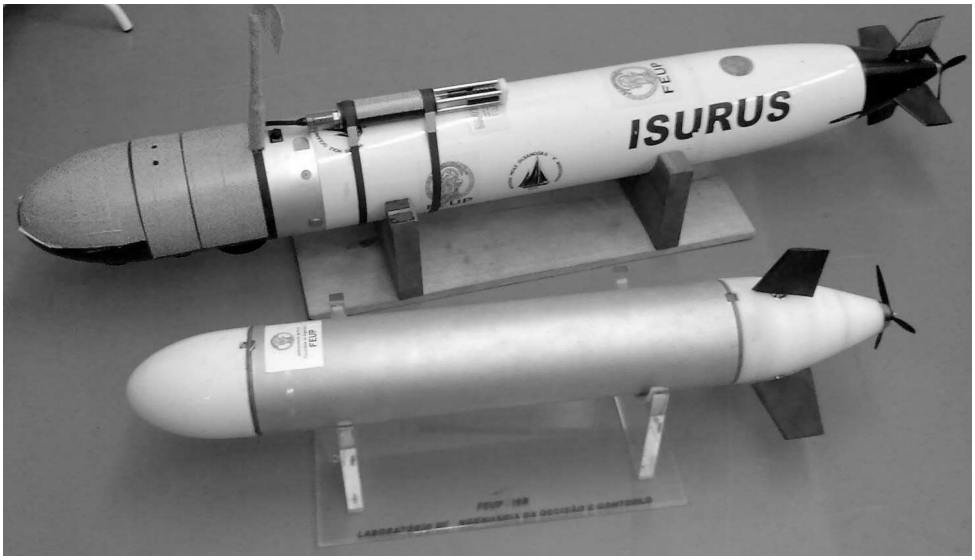

Source: da Silva et al. (2007).

Even though the center of buoyancy is positioned at the origin of the B-frame and the center of gravity is offset $g_z = 0.01m$ from that, for the sake of simplification we will not consider restoring forces in this model. The construction parameters and dynamic coefficient, summarized in Table 3 and 4, were obtained from the paper of da Silva et al. (2007), who derived the numerical coefficients by theoretical and empirical methods as also by adapting from similar AUVs.

Table 3: Building parameters for the LAUV.

Parameter	Symbol	Value
length [cm]	l	108
diameter [cm]	d	15
mass [kg]	m	18

Source: (da Silva et al., 2007).

As we mentioned before, the simulations were done in three different scenarios, follow-

Table 4: Dynamic coefficients for the LAUV.

Parameter	Symbol	Value
inertia coefficients	M	$\begin{bmatrix} 0.04 & 0 & 0 \\ 0 & 2.1 & 0 \\ 0 & 0 & 2.1 \end{bmatrix}$
linear damping coefficients	D_l	$\begin{bmatrix} 0.3 & 0 & 0 \\ 0 & 9.7 & 0 \\ 0 & 0 & 9.7 \end{bmatrix}$
quadratic damping coefficients	D_q	$\begin{bmatrix} 6 \times 10^{-4} & 0 & 0 \\ 0 & 9.1 & 0 \\ 0 & 0 & 9.1 \end{bmatrix}$

Source: (da Silva et al., 2007).

ing the procedure described in the previous section. In the first scenario we chose a large value for the max angular velocity $\overline{\boldsymbol{\omega}}$ in the domain of interest $\mathcal{X}$ (88) in order to analyze the impact of the size of this region. In contrast to scenario one, we limited $\overline{\boldsymbol{\omega}}$ to a small value of 1, which is an angular velocity closer to that found on a real application. The third scenario had the same large value of $\overline{\boldsymbol{\omega}}$ from scenario 1, however we multiplied the damping matrix by $D_e = 10$, in order to investigate the impact of errors in the damping coefficients model since it is desired to have the smallest and cheapest sensors in low cost vehicles as the LAUV (da Silva et al., 2007). Table 5 summarizes the scenario parameters.

Table 5: The parameters for each simulation scenario.

Scenario	$\overline{\omega}[rad/s]$	D_e
Scenario 1	100	1
Scenario 2	1	1
Scenario 3	100	10

Source: the author (2018).

The simulation results of this work will be discussed and presented in the next section.

5.3 Numerical Results

The feasibility of the optimization problem is directly related to the size of the domain of interest (DOA) $\mathcal{X}$, which in turn is defined by two parameters, $\overline{\psi}$ and $\overline{\boldsymbol{\omega}}$, maximum rotation angle for which a solution is found and the limit value of angular velocities,

respectively. As defined in the previous section, the simulations will be done in three different scenarios, see Table 5, and follow the instructions listed in Section 5.1.

5.3.1 Scenario 1

In the first scenario we chose a large value of $\overline{\boldsymbol{\omega}} = 100\ rad/s$, which means about 32 revolutions per second, in order to make a loose restriction in the angular velocities. We run the simulation in a range of max rotation angles $\overline{\psi}$, increasing its value gradually, in order to find the max angle for which a solution is found. From Theorem 4.2, it shows that the largest region $\mathcal{X}_d$ where the gain K can be computed is bounded by the values of $-65^\circ \leq \psi \leq 65^\circ$ for $\overline{\omega} = 100$,

$$\mathcal{X}_d = \{\boldsymbol{x} \in \mathbb{R}^6 :\ |\boldsymbol{x}_i| \leq \sin\frac{65\pi}{360},\ 0 \leq \overline{\psi} < \pi,\ \left|\boldsymbol{x}_j\right| \leq 100\}, \tag{133}$$

for $i = 1, 2, 3$ and $j = 4, 5, 6$.

Considering the above domain, the gain $K = YP$ is given by

$$K = 10^4.\begin{bmatrix} -0.0048 & 0.0000 & -0.0000 & -0.0201 & 0.0001 & -0.0000 \\ 0.0038 & -1.7784 & 0.0046 & 0.0149 & -7.5793 & 0.0194 \\ 0.0000 & 0.0046 & -1.8359 & -0.0000 & 0.0197 & -7.6699 \end{bmatrix}. \tag{134}$$

Besides that, from Theorem 4.2, (108) and (110) show that minimizing trace of P implies in maximizing the region of attraction $\mathcal{R}_d$. Moreover, we know that every trajectory of the closed loop system starting in $\mathcal{R}_d$ exponentially approaches the origin.

Table 6: Feasibility, traces of P and evaluated bounds of the estimated region of attraction $\mathcal{R}_d$ by applying Steps 2-3 to scenario 1.

ψ	$trace(P)$	ε_1	ε_2	ε_3	$\boldsymbol{\omega}_1$	$\boldsymbol{\omega}_2$	$\boldsymbol{\omega}_3$
$\overline{\psi} = 45^\circ$	21.5102	0.3907	0.3679	0.3678	6.8056	3.5794	3.6265
$\overline{\psi} = 60^\circ$	12.8472	0.5075	0.4787	0.4787	5.8252	3.1016	3.1192
$\overline{\psi}_{opt} = 65^\circ$	11.1834	0.5446	0.5136	0.5136	6.0199	3.1393	3.1505
$\overline{\psi} > 65^\circ$	$infeasible$						

Source: the author (2018).

Table 6 presents the feasibility along to the trace of P, which was minimized by (132),

and the bounds for each state of $\mathcal{R}_d$ evaluated in simulations run at several max rotation angles $\overline{\psi}$ by the application of Theorem 4.2. Also, it shows that increasing $\overline{\psi}$ up to about 65° resulted in enlarging $\mathcal{R}_d$. The notation $\overline{\psi}_{opt}$ was applied to identify the point where $\mathcal{R}_d$ was maximized.

Next, we made use of Theorem 4.1 with gain (134), in order to investigate a better region of attraction $\mathcal{R}_a$. Again, we performed the simulation in a range of $\overline{\psi}$ and set of numerical results are shown in Table 7. It was identified that with feedback gain K the estimate region of attraction $\mathcal{R}_a$ achieved similar sizes for equals $\overline{\psi}$. However, the region $\mathcal{X}_a$ was extended and could be computed until about $\overline{\psi} = 156°$, which is also the point of maximization. The region $\mathcal{X}_a$ is given by

$$\mathcal{X}_a = \{\boldsymbol{x} \in \mathbb{R}^6 : \ |\boldsymbol{x}_i| \leq \sin\frac{156\pi}{360}, \ |\boldsymbol{x}_j| \leq 100\}, \tag{135}$$

for $i = 1, 2, 3$ and $j = 4, 5, 6$.

Table 7: Feasibility, traces of P and evaluated bounds of the estimated region of attraction $\mathcal{R}_a$ by applying Steps 4-5 to scenario 1.

ψ	$trace(P)$	ε_1	ε_2	ε_3	$\boldsymbol{\omega}_1$	$\boldsymbol{\omega}_2$	$\boldsymbol{\omega}_3$
$\overline{\psi} = 45°$	19.6609	0.3907	0.3907	0.3907	13.2384	30.3510	30.7733
$\overline{\psi} = 60°$	11.6542	0.5074	0.5075	0.5075	14.9384	33.8021	34.1457
$\overline{\psi} = 65°$	10.1212	0.5445	0.5446	0.5446	15.1456	34.3968	34.5759
$\overline{\psi} = 130°$	3.6354	0.9097	0.9099	0.9099	10.9228	25.8677	25.3545
$\overline{\psi}_{opt} = 156.62°$	3.2230	0.9798	0.9773	0.9656	4.6456	11.6410	11.0517
$\overline{\psi} > 156.62°$	$infeasible$						

Source: the author (2018).

Comparing the results presented in Tables 6 and 7 it is clear to see that this approach implied in a substantial improvement. First, the trace of P, which push the progress, was reduced from 11.1834 to 3.2230, followed by considerably advances in enlarging the region $\mathcal{R}_a$ or the bounds of the vector state.

Figures 7 and 8 illustrate in two and three dimensions the estimated regions of attraction $\mathcal{R}_d$ and $\mathcal{R}_a$ of scenario 1, obtained from Theorem 4.2 and 4.1, respectively. In the top left of both, a three dimensional graph, which axes represent the components of the vector state ε or $\boldsymbol{\omega}$, shows in a spherical volume the bounds presented in Table 7 that limit the estimate region of attraction $\mathcal{R}_a$ in terms of which state. In its turn,

the dotted line depicts the region $\mathcal{X}_a$. The other three graphs, in the top right, bottom left and right, clarify in two dimensions the top, side and front views the 3D region $\mathcal{R}_a$, respectively, including a comparison to the estimate region of attraction $\mathcal{R}_d$, numerically shown in Table 6.

Figure 7: 2D and 3D projection of the estimated region of attraction $\mathcal{R}_a$ and $\mathcal{R}_d$ for vector state ε in Scenario 1.

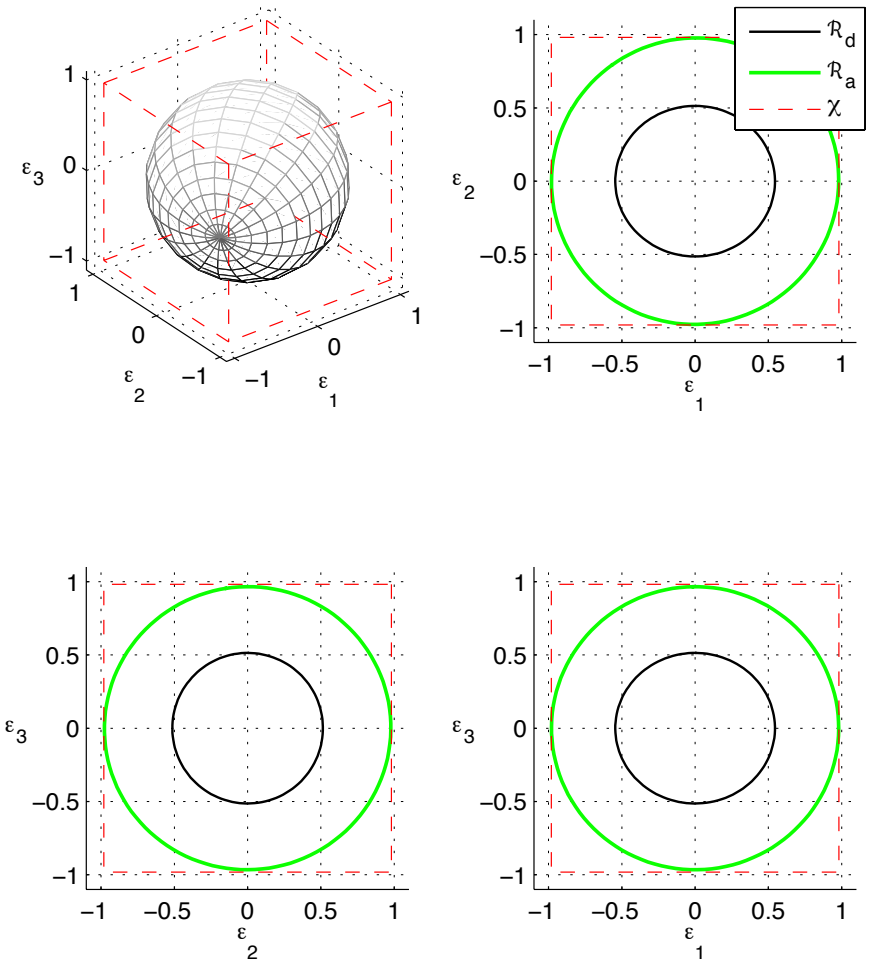

Source: the author (2018).

Even with the small decreased in the range of $\boldsymbol{\omega}_1$, Figure 8, looking at whole results suggests that by the proposed procedure we managed to achieve a considerable increase in the size of the region of attraction leaving little room for improvement of ψ.

Figure 8: 2D and 3D projection of the estimated region of attraction $\mathcal{R}_a$ and $\mathcal{R}_d$ for vector state $\boldsymbol{\omega}$ in Scenario 1.

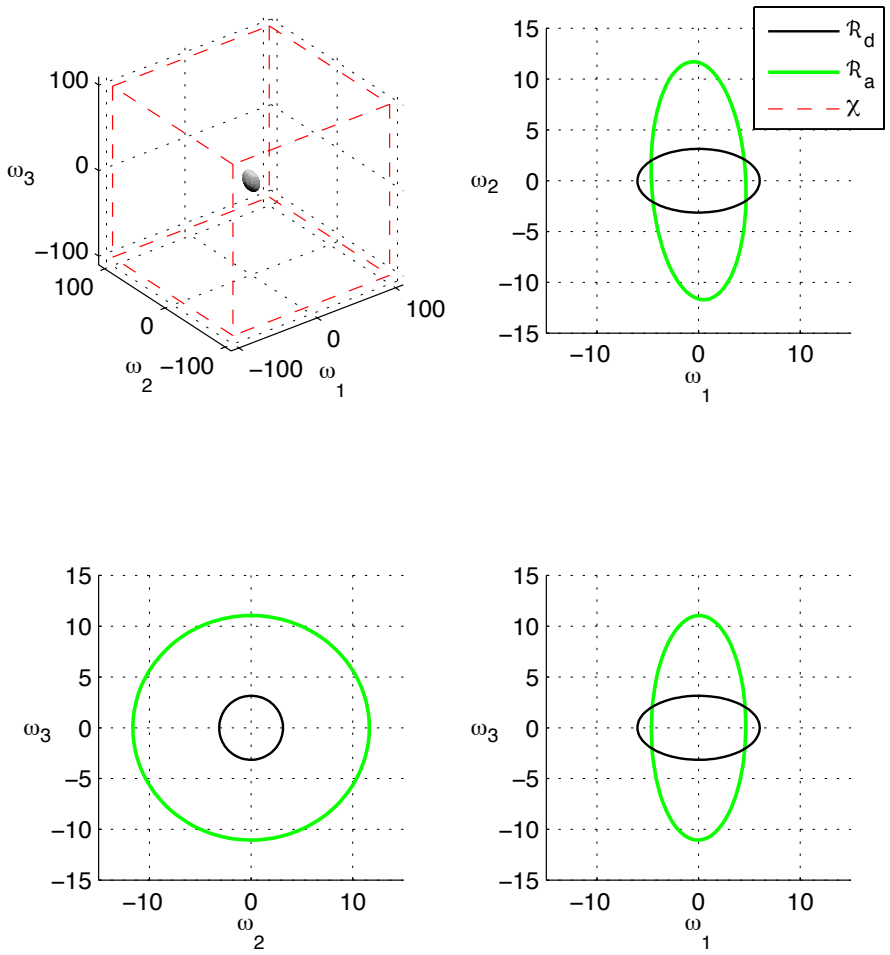

Source: the author (2018).

In Figure 8, the two dimensional plots are zoomed for better understanding of the graph, hence the region $\mathcal{X}_a$ cannot be seen.

5.3.2 Scenario 2

We explored in the second scenario the restriction of the angular velocities to $|\overline{\boldsymbol{\omega}}| \leq 1$ rad/s, which is a value much more closer to the found in real applications. The same procedure followed by scenario one was applied then and the numerical results presented in Table 8, which shows some of the same points presented in Table 6, for enabling comparisons.

Table 8: Feasibility, traces of P and evaluated bounds of the estimated region of attraction $\mathcal{R}_d$ by applying Steps 2-3 to scenario 2.

ψ	$trace(P)$	ε_1	ε_2	ε_3	$\boldsymbol{\omega}_1$	$\boldsymbol{\omega}_2$	$\boldsymbol{\omega}_3$
$\overline{\psi} = 45^\circ$	247.6925	0.3327	0.0986	0.0986	0.8488	0.2524	0.2524
$\overline{\psi} = 60^\circ$	163.4155	0.3769	0.1276	0.1275	0.7410	0.2516	0.2513
$\overline{\psi} = 65^\circ$	145.2605	0.3978	0.1376	0.1375	0.7290	0.2528	0.2525
$\overline{\psi} = 80^\circ$	80.5116	0.4988	0.1950	0.1950	0.7667	0.3002	0.3002
$\overline{\psi} = 90^\circ$	14.3041	0.6317	0.5356	0.5356	0.8847	0.7508	0.7507
$\overline{\psi}_{opt} = 95.9^\circ$	12.3139	0.6553	0.5995	0.5996	0.8742	0.8017	0.8015
$\overline{\psi} = 96.5^\circ$	13.5649	0.6238	0.5728	0.5729	0.8287	0.7621	0.7620
$\overline{\psi} = 97.1^\circ$	25.8601	0.4552	0.4146	0.4147	0.6022	0.5487	0.5488
$\overline{\psi} > 97.1^\circ$	$infeasible$						

Source: the author (2018).

Even though solutions were found until around $\overline{\psi} = 97^\circ$, this time we opted for restricting the domain of interest $\mathcal{X}_d$ up to 95.9°, because it produced a larger region of attraction $\mathcal{R}_d$. The domain of interested is given by

$$\mathcal{X}_d = \{\boldsymbol{x} \in \mathbb{R}^6 : \ |\boldsymbol{x}_i| \leq \sin\frac{95.9\pi}{360}, \ \left|\boldsymbol{x}_j\right| \leq 1\}, \tag{136}$$

for $i = 1, 2, 3$ and $j = 4, 5, 6$.

By narrowing the domain $\mathcal{X}_d$ to the above, the feedback gain K obtained at $\overline{\psi} = 95.9^\circ$ is equals to

$$K = 10^5. \begin{bmatrix} -0.0323 & -0.0000 & 0.0000 & -0.0502 & -0.0000 & 0.0000 \\ -0.0000 & -3.8468 & 0.0000 & -0.0000 & -5.3271 & 0.0000 \\ 0.0000 & -0.0000 & -3.8476 & 0.0000 & -0.0000 & -5.3287 \end{bmatrix}. \tag{137}$$

Given the above feedback gain computed from $\mathcal{X}_d$, we applied it to Theorem 4.2 in order to search for a larger region of attraction. The results can be read in Table 9.

Table 9: Feasibility, traces of P and evaluated bounds of the estimated region of attraction $\mathcal{R}_a$ by applying Steps 4-5 to scenario 2.

ψ	$trace(P)$	ε_1	ε_2	ε_3	$\boldsymbol{\omega}_1$	$\boldsymbol{\omega}_2$	$\boldsymbol{\omega}_3$
$\overline{\psi} = 45^\circ$	24.4314	0.3785	0.3751	0.3751	0.9686	0.9600	0.9600
$\overline{\psi} = 60^\circ$	16.7138	0.4802	0.4726	0.4726	0.9461	0.9312	0.9312
$\overline{\psi} = 65^\circ$	15.2957	0.5106	0.5012	0.5012	0.9376	0.9203	0.9203
$\overline{\psi} = 80^\circ$	12.6979	0.5908	0.5742	0.5742	0.9096	0.8842	0.8842
$\overline{\psi} = 90^\circ$	11.8011	0.6345	0.6121	0.6121	0.8896	0.8582	0.8582
$\overline{\psi} = 95.9^\circ$	11.4665	0.6568	0.6304	0.6305	0.8776	0.8424	0.8424
$\overline{\psi} = 110^\circ$	11.0677	0.6994	0.6630	0.6630	0.8492	0.8049	0.8050
$\overline{\psi} = 120^\circ$	10.9994	0.7221	0.6691	0.6692	0.8297	0.7953	0.7953
$\overline{\psi}_{opt} = 131^\circ$	10.9800	0.7401	0.6696	0.6697	0.8102	0.7942	0.7942
$\overline{\psi} = 140^\circ$	10.9826	0.7419	0.6696	0.6696	0.8077	0.7940	0.7940
$\overline{\psi} = 170^\circ$	10.9972	0.7392	0.6697	0.6698	0.8098	0.7927	0.7927
$\overline{\psi} = 177.9^\circ$	249.2390	0.1597	0.2183	0.2190	0.1041	0.1620	0.1625
$\overline{\psi} > 177.9^\circ$	$infeasible$						

Source: the author (2018).

The solver was able to find a solution for up to about $\overline{\psi} = 178^\circ$, however the estimate region of attraction $\mathcal{R}_a$ started to decrease for $\overline{\psi} > 131^\circ$. Thus, the domain of interest $\mathcal{X}_a$ is given by

$$\mathcal{X}_a = \{\boldsymbol{x} \in \mathbb{R}^6 : \ |\boldsymbol{x}_i| \leq \sin\frac{131\pi}{360}, \ \left|\boldsymbol{x}_j\right| \leq 1\}, \tag{138}$$

for $i = 1, 2, 3$ and $j = 4, 5, 6$.

Also, comparing Table 8 and 9 it shows that by narrowing the bounds of the angular velocities, the solver achieved great improvements in the size of $\mathcal{R}_a$ for the former angles $\overline{\psi}$, however it did not accomplish expressive results at optimal points.

Additionally, it is possible to see at $\overline{\psi} = 177.9^\circ$ how hard the solver worked to find a solution even penalizing the size of the estimate region of attraction.

Figures 9 and 10 show the resemblance between the numerical results presented in Tables 8 and 9 through graphs of similar size and shape of the estimate region of attraction $\mathcal{R}_d$ and $\mathcal{R}_d$ when the gain (137) is applied at $\overline{\psi} = 131^\circ$. We can conclude that the estimate

region of attraction was almost maximized just after Steps 2-3.

Figure 9: 2D and 3D projection of the estimated region of attraction $\mathcal{R}_a$ and $\mathcal{R}_d$ for vector state ε in Scenario 2.

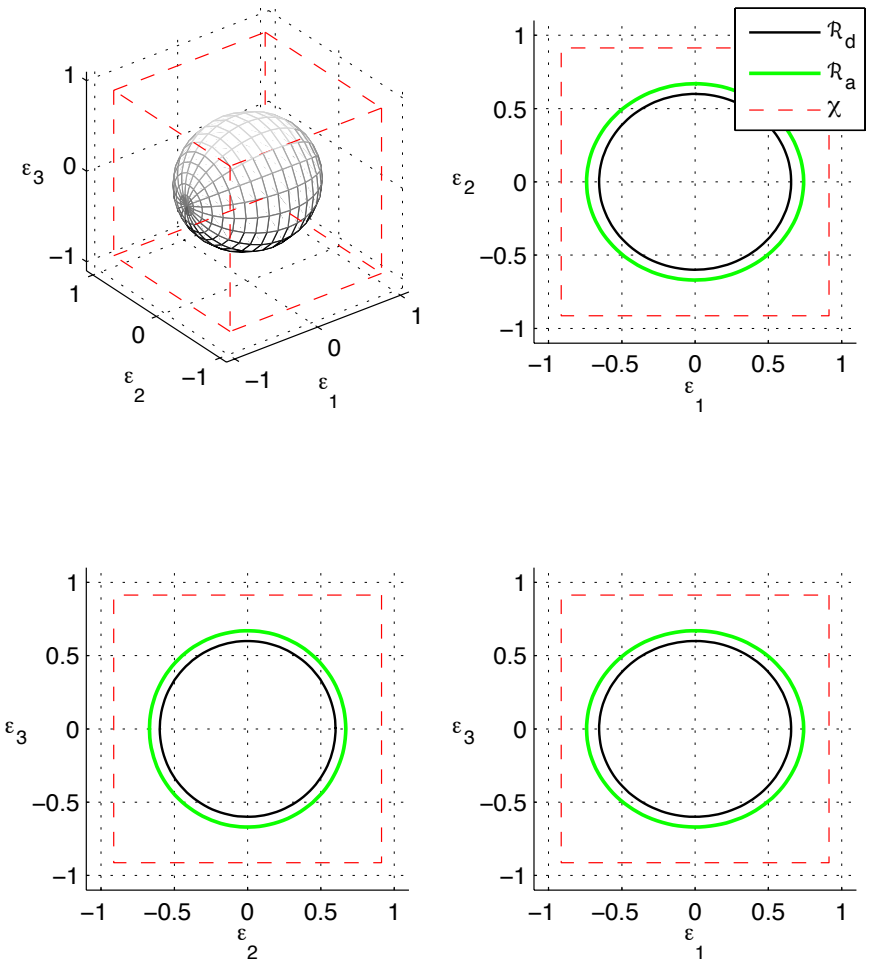

Source: the author (2018).

In the context of the Light Autonomous Underwater Vehicle application we understand that disturbances and input signals acting on the vehicle that do not surpass the boarder of the region of attraction $\mathcal{R}_a$ will be leaded to the equilibrium point when $t \to \infty$.

Figure 10: 2D and 3D projection of the estimated region of attraction $\mathcal{R}_a$ and $\mathcal{R}_d$ for vector state $\boldsymbol{\omega}$ in Scenario 2.

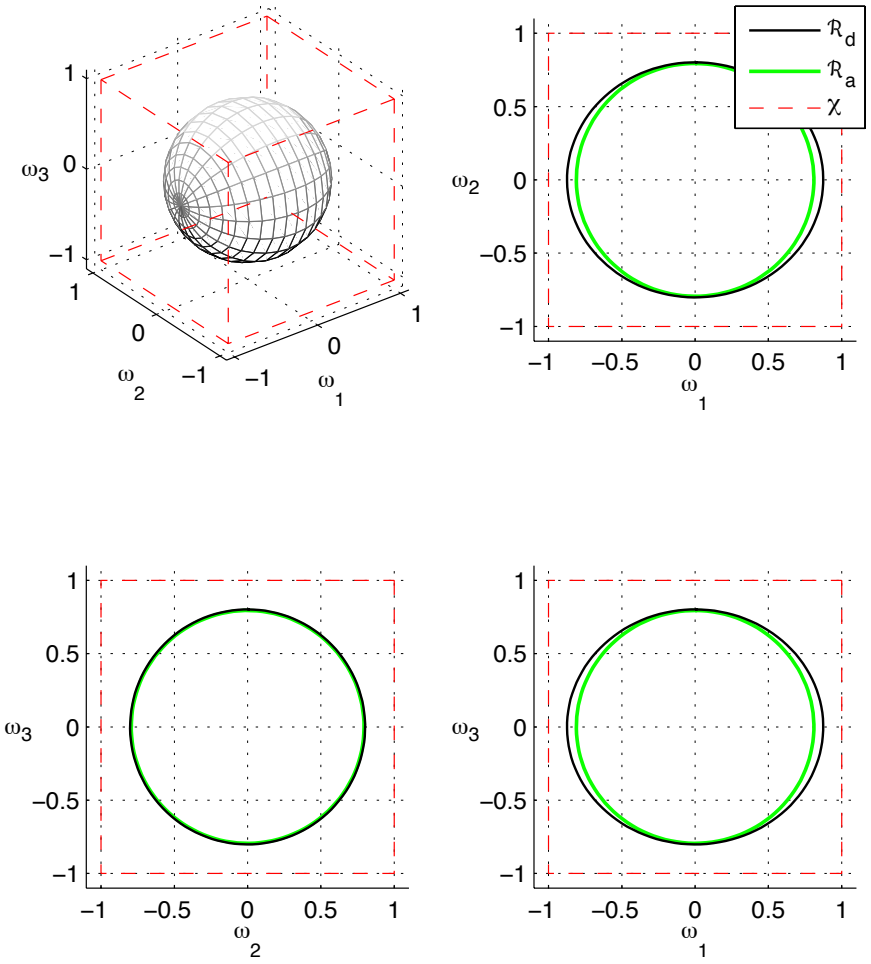

Source: the author (2018).

5.3.3 Scenario 3

The third scenario was proposed to investigate the impact of modeling error of damping coefficients. From (58) and (50) we know that the damping effect is the joint of potential damping, skin friction, wave drift damping and damping due to vortex shedding, therefore coefficients that must be modeled and experimented in order to respond similarly to the real dynamics of the vehicle. Considering that the Light Autonomous Underwater Vehicle is a low cost vehicle comparing to a regular AUV, it is interesting to use the smallest and cheapest set of sensors available, what may result in a not so precise modeling.

In the light of these considerations, we multiplied by 10 the coefficients of the damping matrix $D(\boldsymbol{\omega})$, which is composed by linear and quadratic terms, then executed all the procedures described in Section 5.1. For the Steps 2-3, the numerical results are shown in Table 10.

Table 10: Feasibility, traces of P and evaluated bounds of the estimated region of attraction $\mathcal{R}_d$ by applying Steps 2-3 to scenario 3.

ψ	$trace(P)$	ε_1	ε_2	ε_3	$\boldsymbol{\omega}_1$	$\boldsymbol{\omega}_2$	$\boldsymbol{\omega}_3$
$\overline{\psi} = 45^\circ$	38.6871	0.3907	0.3734	0.3734	0.7134	0.3570	0.3539
$\overline{\psi} = 50^\circ$	33.7791	0.4305	0.4117	0.4117	0.6688	0.3754	0.3713
$\overline{\psi} = 55^\circ$	24.4651	0.4695	0.4483	0.4483	0.7618	0.4944	0.4902
$\overline{\psi}_{opt} = 57.95^\circ$	22.0769	0.4920	0.4678	0.4678	0.8624	0.5189	0.5165
$\overline{\psi} > 57.95^\circ$	$infeasible$						

Source: the author (2018).

We found that there is no solution for about $\overline{\psi} > 57.95^\circ$, which is also the optimal solution point. The region $\mathcal{X}_a$ is given by

$$\mathcal{X}_d = \{\boldsymbol{x} \in \mathbb{R}^6 : \ |\boldsymbol{x}_i| \leq \sin\frac{57.95\pi}{360}, \ \left|\boldsymbol{x}_j\right| \leq 100\}, \tag{139}$$

for $i = 1, 2, 3$ and $j = 4, 5, 6$.

At the optimal point, the computed feedback gain is

$$K = 10^4. \begin{bmatrix} -0.0001 & -0.0000 & -0.0000 & -0.0137 & 0.0000 & -0.0000 \\ 0.0000 & -0.0068 & 0.0000 & 0.0035 & -6.3805 & 0.0197 \\ -0.0000 & 0.0000 & -0.0068 & -0.0004 & 0.0196 & -6.4436 \end{bmatrix}. \tag{140}$$

Through the application of Theorem 4.1 with gain (140) we investigated a larger region of attraction $\mathcal{R}_a$ and presented the estimations in Table 11 for some values of $\overline{\psi}$.

Table 11: Feasibility, traces of P and evaluated bounds of the estimated region of attraction $\mathcal{R}_a$ by applying Steps 4-5 to scenario 3.

ψ	$trace(P)$	ε_1	ε_2	ε_3	$\boldsymbol{\omega}_1$	$\boldsymbol{\omega}_2$	$\boldsymbol{\omega}_3$
$\overline{\psi} = 45^\circ$	19.8040	0.3907	0.3907	0.3907	3.0761	6.3860	6.4964
$\overline{\psi} = 50^\circ$	16.3413	0.4305	0.4305	0.4305	3.0563	6.4557	6.4919
$\overline{\psi} = 55^\circ$	13.7774	0.4695	0.4695	0.4695	3.0994	5.6561	5.7176
$\overline{\psi} = 57.95^\circ$	12.6305	0.4920	0.4920	0.4920	3.2163	3.7293	3.7633
$\overline{\psi} = 80^\circ$	9.2464	0.4871	0.6494	0.6494	2.9922	3.3309	3.3652
$\overline{\psi} = 90^\circ$	8.5482	0.4815	0.7132	0.7132	2.8492	3.3074	3.3429
$\overline{\psi} = 110^\circ$	7.9115	0.4655	0.8241	0.8241	2.5010	3.2065	3.2560
$\overline{\psi}_{opt} = 118^\circ$	7.8631	0.4571	0.8616	0.8616	2.3280	3.1433	3.2156
$\overline{\psi} = 130^\circ$	7.9850	0.4422	0.9100	0.9100	2.0183	3.0354	3.1294
$\overline{\psi} = 156.4^\circ$	10.7128	0.3849	0.9762	0.9806	0.8127	2.3638	2.3495
$\overline{\psi} > 156.4^\circ$	$infeasible$						

Source: the author (2018).

Again, the size of the estimate region of attraction $\mathcal{R}_a$ increased up to a point and then started to decreased until about $\overline{\psi} > 156.4^\circ$, from where the solver stopped to finding solutions, see Table 11.

The achieved rotation span were the region of attraction is optimized better is represented by the domain

$$\mathcal{X}_a = \{\boldsymbol{x} \in \mathbb{R}^6 : \ |\boldsymbol{x}_i| \leq \sin\frac{118\pi}{360}, \ |\boldsymbol{x}_j| \leq 100\}, \tag{141}$$

for $i = 1, 2, 3$ and $j = 4, 5, 6$.

From Figure 11, we see that the region of attraction is tightly bounded by $\mathcal{X}_a$ in the states ε_2 and ε_3, leaving little room for improvement. As the LAUV is a torpedo shaped vehicle, which its main rotation movements are pitch and yaw, we may conclude that the shape of the estimate region of attraction $\mathbb{R}_a$ is attributed to constructive specification, thus the largest rotation span is set around the axes Y_{RB} and Z_{RB}.

Figure 11: 2D and 3D projection of the estimated region of attraction $\mathcal{R}_a$ and $\mathcal{R}_d$ for vector state ε in Scenario 3.

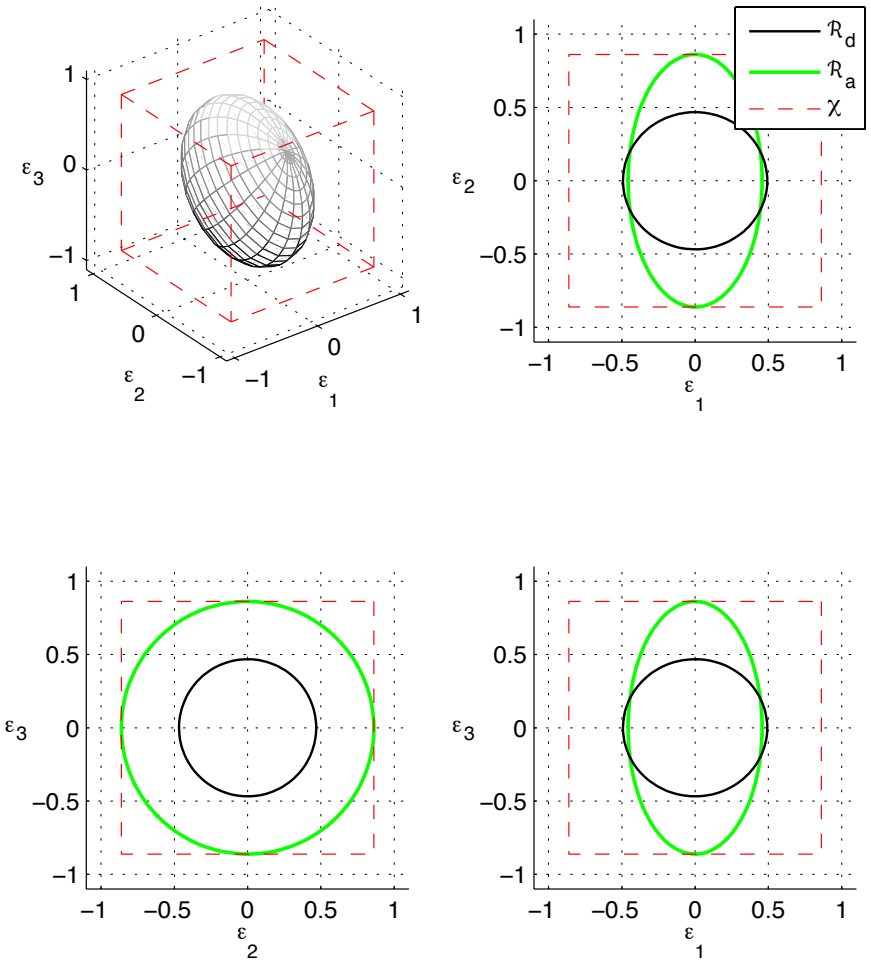

Source: the author (2018).

After all, we concluded that substantial results may be achieved by the application of the proposed method. In the first and third scenarios, great results were achieved, enlarging considerably the estimate region of attraction $\mathcal{R}_a$ in comparison to $\mathcal{R}_d$, while in the second scenario the estimate region of attraction had being almost maximized by Steps 2-3.

Figure 12: 2D and 3D projection of the estimated region of attraction $\mathcal{R}_a$ and $\mathcal{R}_d$ for vector state $\boldsymbol{\omega}$ in Scenario 3.

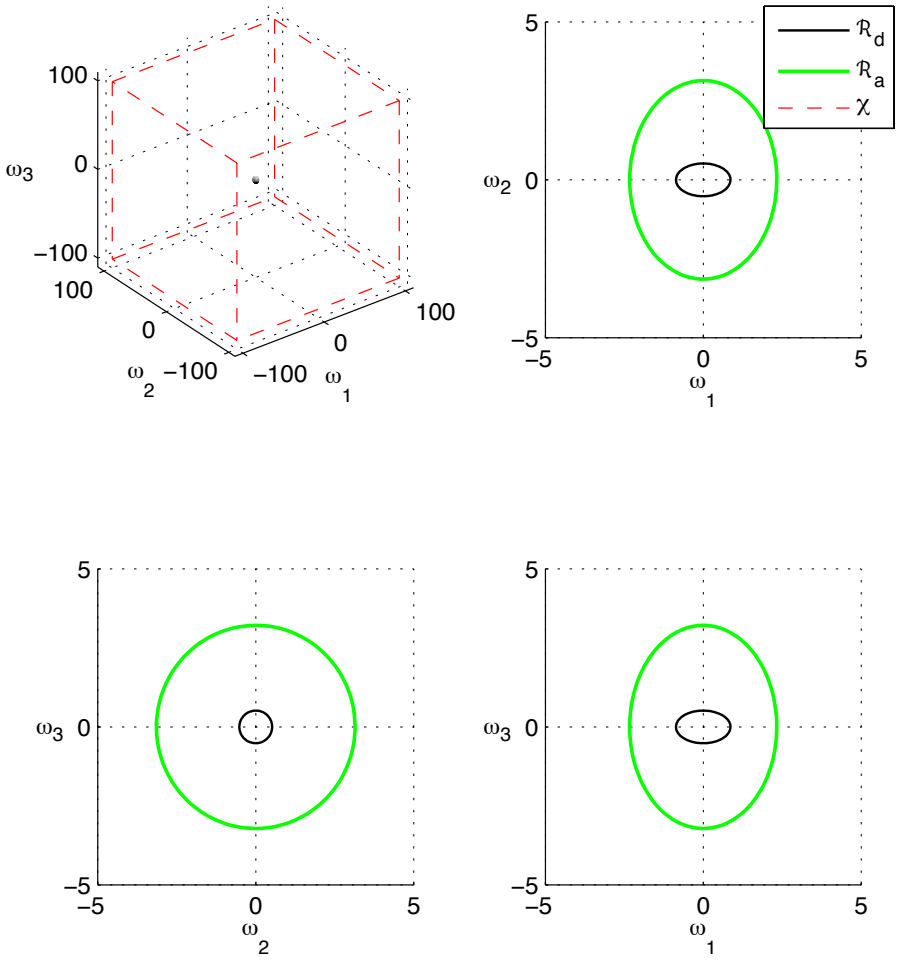

Source: the author (2018).

6 Conclusion

Underwater robotics is a huge area of research evidenced by the substantial quantity of publications and techniques that have being developed. Also, it is an extremely important topic that has being little explored considering that the ocean covers about two-thirds of the earth (Yuh, 2000). Autonomous Underwater Vehicles have many and diverse applications, from science to military, as shown in Section 1, and torpedo shaped is one of the most typical designs.

This work addresses important concepts in the design of controllers. The vehicle dynamic model approach in this work is very similar to the Spacecraft approached by Salton et al. (2017) and extended here for AUVs. Given this representation, it opens space for implementing a series of linear-like tools that potentially enriches the task of control designing.

Also, given the DAR representation, the control and analysis task was cast as a semidefinite optimization problem. In three scenarios we compute the feedback gain K that optimize the region of attraction and the numerical results were discusses in Section 5. From now, a series of other experiments may be studied and advance this work.

6.1 Suggestions for Future Work

Once the Differential Algebraic Representation of the Autonomous Underwater Vehicle is described, a set of investigations may be subsequently done. Input saturation may be added by extending the Theorem 4.2, following the idea presented by Oliveira et al. (2012). Also, this model may be better explored if considering the restoring forces. Moreover, the application of this strategy for describing all equations of motion in DAR, also considering the translational movements, will be considered along to the evaluation of the Jacobian Matrix 66 that relates the inputs with the torques as presented in da Silva et al. (2007).

References

Anastassiu, H. T., Atlamazoglou, P. E., and Kaklamani, D. I. (2003). Application of bicomplex (quaternion) algebra to fundamental electromagnetics: a lower order alternative to the helmholtz equation. *IEEE Transactions on Antennas and Propagation*, 51(8):2130–2136.

Bessa, W. M., Dutra, M. S., and Kreuzer, E. (2010). An adaptive fuzzy sliding mode controller for remotely operated underwater vehicles. *Robotics and Autonomous Systems*, 58(1):16–26.

Black, M. R. and Butler, B. (1994). Arctic ocean trials of trackpoint ultrashort baseline acoustic positioning systems. In *Autonomous Underwater Vehicle Technology, 1994. AUV'94., Proceedings of the 1994 Symposium on*, pages 297–302. IEEE.

Blidberg, D. R. and Jalbert, J. (1995). Mission and system sensors. *Underwater Robotic Vehicles: Design and Control*, 1:185–220.

Boyd, S., El Ghaoui, L., Feron, E., and Balakrishnan, V. (1994). *Linear matrix inequalities in system and control theory*, volume 15. Siam.

Boyd, S. and Vandenberghe, L. (2004). *Convex optimization*. Cambridge university press.

Bradley, A. M., Feezor, M. D., Singh, H., and Sorrell, F. Y. (2001). Power systems for autonomous underwater vehicles. *IEEE Journal of oceanic Engineering*, 26(4):526–538.

Chitre, M., Shahabudeen, S., and Stojanovic, M. (2008). Underwater acoustic communications and networking: Recent advances and future challenges. *Marine technology society journal*, 42(1):103–116.

Choi, S. K. and Yuh, J. (1996). Experimental study on a learning control system with bound estimation for underwater robots. In *Underwater Robots*, pages 113–120. Springer.

Coutinho, D. F., Bazanella, A. S., Trofino, A., and e Silva, A. S. (2004). Stability analysis and control of a class of differential-algebraic nonlinear systems. *International Journal of Robust and Nonlinear Control: IFAC-Affiliated Journal*, 14(16):1301–1326.

Cristi, R., Papoulias, F. A., and Healey, A. J. (1990). Adaptive sliding mode control of autonomous underwater vehicles in the dive plane. *IEEE journal of Oceanic Engineering*, 15(3):152–160.

Cui, R., Li, Y., and Yan, W. (2016). Mutual information-based multi-auv path planning for scalar field sampling using multidimensional rrt. *IEEE Transactions on Systems, Man, and Cybernetics: Systems*, 46(7):993–1004.

Cui, R., Yang, C., Li, Y., and Sharma, S. (2017). Adaptive neural network control of auvs with control input nonlinearities using reinforcement learning. *IEEE Transactions on Systems, Man, and Cybernetics: Systems*, 47(6):1019–1029.

da Silva, J. E., Terra, B., Martins, R., and de Sousa, J. B. (2007). Modeling and simulation of the lauv autonomous underwater vehicle. In *13th IEEE IFAC International Conference on Methods and Models in Automation and Robotics*. Szczecin, Poland Szczecin, Poland.

Davies, P. and Rajapakse, Y. D. (2014). *Durability of composites in a marine environment*, volume 208. Springer.

DeBitetto, P. A. (1995). Fuzzy logic for depth control of unmanned undersea vehicles. *IEEE journal of oceanic engineering*, 20(3):242–248.

Diebel, J. (2006). Representing attitude: Euler angles, unit quaternions, and rotation vectors. *Matrix*, 58(15-16):1–35.

Fossen, T. I. et al. (1994). *Guidance and control of ocean vehicles*, volume 199. Wiley New York.

Goheen, K. R. and Jefferys, E. R. (1990). Multivariable self-tuning autopilots for autonomous and remotely operated underwater vehicles. *IEEE Journal of Oceanic Engineering*, 15(3):144–151.

Hamilton, W. R. (1844). Ii. on quaternions; or on a new system of imaginaries in algebra. *The London, Edinburgh, and Dublin Philosophical Magazine and Journal of Science*, 25(163):10–13.

Hasvold, Ø., Størkersen, N. J., Forseth, S., and Lian, T. (2006). Power sources for autonomous underwater vehicles. *Journal of Power Sources*, 162(2):935–942.

Healey, A. J. and Lienard, D. (1993). Multivariable sliding mode control for autonomous diving and steering of unmanned underwater vehicles. *IEEE journal of Oceanic Engineering*, 18(3):327–339.

Ishaque, K., Abdullah, S. S., Ayob, S. M., and Salam, Z. (2010). Single input fuzzy logic controller for unmanned underwater vehicle. *Journal of Intelligent and Robotic Systems*, 59(1):87–100.

Isokawa, T., Kusakabe, T., Matsui, N., and Peper, F. (2003). Quaternion neural network and its application. In *International Conference on Knowledge-Based and Intelligent Information and Engineering Systems*, pages 318–324. Springer.

Joshi, S. and Talange, D. (2016). Fault tolerant control of an auv using periodic output feedback with multi model approach. *International Journal of System Dynamics Applications (IJSDA)*, 5(2):41–62.

Khalil, H. K. (1996). Noninear systems. *Prentice-Hall, New Jersey*, 2(5):5–1.

Lewis, E. V. (1989). Principles of naval architecture–second revision. *The Society of Naval Architects and Marine Engineers, New Jersey.*

Liang, X., Zhang, J., Qin, Y., and Yang, H. (2013). Dynamic modeling and computer simulation for autonomous underwater vehicles with fins. *JCP*, 8(4):1058–1064.

Lofberg, J. (2004). Yalmip: A toolbox for modeling and optimization in matlab. In *Computer Aided Control Systems Design, 2004 IEEE International Symposium on*, pages 284–289. IEEE.

Lorentz, J. and Yuh, J. (1996). A survey and experimental study of neural network auv control. In *Autonomous Underwater Vehicle Technology, 1996. AUV'96., Proceedings of the 1996 Symposium on*, pages 109–116. IEEE.

Murray, R. M. (2017). *A mathematical introduction to robotic manipulation*. CRC press.

Nakamura, Y. and Savant, S. (1992). Nonlinear tracking control of autonomous underwater vehicles. In *Robotics and Automation, 1992. Proceedings., 1992 IEEE International Conference on*, pages A4–A9. IEEE.

Oliveira, M., da Silva, J. G., and Coutinho, D. (2012). State feedback design for rational nonlinear control systems with saturating inputs. In *American Control Conference (ACC), 2012*, pages 2331–2336. IEEE.

Paull, L., Saeedi, S., Seto, M., and Li, H. (2014). Auv navigation and localization: A review. *IEEE Journal of Oceanic Engineering*, 39(1):131–149.

Pettersen, K. and Egeland, O. (1996). Position and attitude control of an underactuated autonomous underwater vehicle. In *IEEE Conference on Decision and Control*, volume 1, pages 987–991. INSTITUTE OF ELECTRICAL ENGINEERS INC (IEE).

Podder, T. K., Antonelli, G., and Sarkar, N. (2001). An experimental investigation into the fault-tolerant control of an autonomous underwater vehicle. *Advanced Robotics*, 15(5):501–520.

Sagatun, S. (1992). Modeling and control of underwater vehicles: A lagrangian approach. *Norwegian Institute of Technology*.

Sahu, B. K. and Subudhi, B. (2014). Adaptive tracking control of an autonomous underwater vehicle. *International Journal of Automation and Computing*, 11(3):299–307.

Salton, A. T., Castro, R. S., Borges, B. S., Flores, J. V., and Coutinho, D. F. (2017). Semidefinite programming solution to the spacecraft analysis and control problem. *IFAC-PapersOnLine*, 50(1):3959–3964.

Scherer, C. and Weiland, S. (2004). *Linear matrix inequalities in control*. Dutch Institute of Systems and Control (DISC).

Shukla, A. and Karki, H. (2016). Application of robotics in offshore oil and gas industry—a review part ii. *Robotics and Autonomous Systems*, 75:508–524.

Silva, J. and Sousa, J. (2008). Models for simulation and control of underwater vehicles. In *New Approaches in Automation and Robotics*. InTech.

Tabaii, S. S., El-Hawary, F., and El-Hawary, M. (1994). Hybrid adaptive control of autonomous underwater vehicle. In *Autonomous Underwater Vehicle Technology, 1994. AUV'94., Proceedings of the 1994 Symposium on*, pages 275–282. IEEE.

Toh, K.-C., Todd, M. J., and Tütüncü, R. H. (1999). Sdpt3—a matlab software package for semidefinite programming, version 1.3. *Optimization methods and software*, 11(1-4):545–581.

Triantafyllou, M. and Amzallag, A. (1984). A new generation of underwater unmanned tethered vehicles carrying heavy equipment at large depths. Technical report, Technical Report MITSG 85-30TN, MIT Dea Grant, Boston, MA.

Trofino, A. (2000). Robust stability and domain of attraction of uncertain nonlinear systems. In *American Control Conference, 2000. Proceedings of the 2000*, volume 5, pages 3707–3711. IEEE.

Trofino, A. and Dezuo, T. (2014). Lmi stability conditions for uncertain rational nonlinear systems. *International Journal of Robust and Nonlinear Control*, 24(18):3124–3169.

Tsukamoto, C., Lee, W., Yuh, J., Choi, S. K., and Lorentz, J. (1997). Comparison study on advanced thruster control of underwater robots. In *Robotics and Automation, 1997. Proceedings., 1997 IEEE International Conference on*, volume 3, pages 1845–1850. IEEE.

Turner, M. C. and Bates, D. G. (2007). Mathematical methods for robust and nonlinear control. *Book series on control systems. Springer, Berlin.*

Walton, J., Cooke, M., and Uhrich, R. (1993). Advanced unmanned search system. Technical report, NAVAL COMMAND CONTROL AND OCEAN SURVEILLANCE CENTER RDT AND E DIV SAN DIEGO CA.

Xiang, X., Yu, C., and Zhang, Q. (2017). Robust fuzzy 3d path following for autonomous underwater vehicle subject to uncertainties. *Computers & Operations Research*, 84:165–177.

Yang, K. C., Yuh, J., and Choi, S. K. (1998). Experimental study of fault-tolerant system design for underwater robots. In *Robotics and Automation, 1998. Proceedings. 1998 IEEE International Conference on*, volume 2, pages 1051–1056. IEEE.

Yoerger, D. and Slotine, J. (1985). Robust trajectory control of underwater vehicles. *IEEE Journal of Oceanic Engineering*, 10(4):462–470.

Yuh, J. (1990a). Modeling and control of underwater robotic vehicles. *IEEE Transactions on Systems, man, and Cybernetics*, 20(6):1475–1483.

Yuh, J. (1990b). A neural net controller for underwater robotic vehicles. *IEEE Journal of Oceanic Engineering*, 15(3):161–166.

Yuh, J. (2000). Design and control of autonomous underwater robots: A survey. *Autonomous Robots*, 8(1):7–24.

Yuh, J., Marani, G., and Blidberg, D. R. (2011). Applications of marine robotic vehicles. *Intelligent service robotics*, 4(4):221.

Pontifícia Universidade Católica do Rio Grande do Sul
Pró-Reitoria de Graduação
Av. Ipiranga, 6681 - Prédio 1 - 3º. andar
Porto Alegre - RS - Brasil
Fone: (51) 3320-3500 - Fax: (51) 3339-1564
E-mail: prograd@pucrs.br
Site: www.pucrs.br